# Post-production modifications of murine mesenchymal stem cell (mMSC) derived extracellular vesicles (EVs) and impact on their cellular interaction

Sarah Le Saux, Hanna Aarrass, Josephine Lai Kee Him, Patrick Bron, Jean Armengaud, Guylaine Miotello, Justine Bertrand-Michel, Emeric Dubois, Simon George, Orestis Faklaris, et al.

# Post-production modifications of murine Mesenchymal Stem Cell (mMSC) derived Extracellular Vesicles (EVs) and impact on their cellular interaction

Sarah LE SAUX[1], Hanna AARRASS[1], Joséphine LAI-KEE-HIM[2], Patrick BRON[2], Jean ARMENGAUD[3], Guylaine MIOTELLO[3], Justine BERTRAND-MICHEL[4], Emeric DUBOIS[5], Simon GEORGE[5], Orestis FAKLARIS[6], Jean-Marie DEVOISSELLE[1], Philippe LEGRAND[1], Joël CHOPINEAU[1, 7], Marie MORILLE[1*]

[1] ICGM, Univ Montpellier, ENSCM, CNRS, Montpellier, France;
[2] CBS, Univ Montpellier, INSERM, CNRS, Montpellier, France;
[3] Laboratory « Innovative technologies for Detection and Diagnostics », CEA-Marcoule, DRF/JOLIOT/DMTS/SPI/Li2D, Bagnols-sur-Cèze, France;
[4] MetaToul-LIPIDOMIQUE, Institut des Maladies Métaboliques et Cardiovasculaires (I2MC) Inserm/Université Paul Sabatier UMR1048, Toulouse, France;
[5] MGX-Montpellier GenomiX, IGF, CNRS, INSERM, Univ Montpellier, Montpellier;
[6] Montpellier Ressources Imagerie, Biocampus, CNRS, INSERM, Univ Montpellier, Montpellier;
[7] Université de Nîmes, Nîmes, France.

* corresponding author: marie.morille@umontpellier.fr

## Abstract

In regards to their key role in intercellular communication, extracellular vesicles (EVs) have a strong potential as bio-inspired drug-delivery systems. With the aim of circumventing some of their well-known issues (production yield, drug loading yield, pharmacokinetics), we specifically focused on switching the biological vision of these entities to a more physico-chemical one, and to consider and fine-tune EVs as synthetic vectors. To allow a rational use, we first performed a full physico-chemical (size, concentration, surface charge, cryoTEM), biochemical (western blot, proteomics, lipidomics, transcriptomics) and biological (cell internalisation) characterisation of murine mesenchymal stem cell (mMSC)-derived EVs. A stability study based on evaluating the colloidal behaviour of obtained vesicles was performed in order to identify optimal storage conditions. We evidenced the interest of using EVs instead of liposomes, in regards to target cell internalisation efficiency. EVs were shown to be internalised through a caveolae and cholesterol-dependent pathway, following a different endocytic route than liposomes. Then, we characterised the effect of physical methods scarcely investigated with EVs (extrusion through 50 nm membranes, freeze-drying, sonication) on EV size, concentration, structure and cell internalisation properties. Our extensive characterisation of the effect of these physical processes highlights their promise as loading methods to make EVs efficient delivery vehicles.

## Keywords

Extracellular vesicles, Drug delivery system, Post-production modifications, physical modifications, exosomes, Endocytosis pathway

## 1. Introduction

The unveiling of the natural vectorisation capabilities of extracellular vesicles (EVs) highlights them as potential alternative to synthetic vectors for the transport of versatile molecules toward cells [1]. EVs are commonly classified in three subcategories: (i) apoptotic bodies (diameter range 1 – 5 μm) produced during apoptosis; (ii) microvesicles (100 nm – 1 μm) (MVs), which bud directly from the plasma membrane; (iii) exosomes, the smallest EVs (50-150 nm), which are released by the fusion of multivesicular endosomal bodies with the plasma membrane [2-4]. EVs, especially exosomes, have been described for the past thirty years as key players of cellular communication, shuttling over short and long distances molecules such as lipids, nucleic acids and proteins from one cell to another [4, 5]. Nevertheless, despite convincing *in vivo* results [6-8], EVs still failed to convince the drug delivery scientific community. This could be explained by several "practical" drawbacks such as (i) limited scalability of production and isolation, (ii) lack of standard storage conditions, (iii) heterogeneity of vesicle populations hindering clear EV identification and subsequent behaviour study, (iv) low drug loading efficiency and reproducibility, (v) plasma instability if considered for an intravenous non autologous administration. These EV flaws might be overcome by switching the biological vision of these entities to a more physico-chemical one. Illustrating this, two main strategies have been carried out to allow drug loading into EVs: (i) modifying producing cells in order to obtain modified EVs, which can be called 'pre-production modifications' relying on biological expertise or (ii) modifying EVs after isolation or 'post-production modifications' relying on physico-chemical methods. In the beginning of the 2010s, many teams initially focused on pre-production modifications; these proved feasible but could be burdensome and time-consuming [1]. Furthermore, standardizing the amount of modified EVs produced from modified cells is challenging, which makes the efficiency and reproducibility of these pre-production methods difficult to control. Post-production modifications were also explored, with a majority of teams using passive methods such as co-incubation, or an active method, electroporation, as cargo loading protocols. However, incubation seems to allow loading of a low variety of contents and it is mainly adapted for small, hydrophobic molecules [1, 9]. While mainly used in the first studies, electroporation has been reported to cause cargo aggregation, especially with nucleic acids [10]. Other physico-chemical methods such as extrusion and sonication [2, 11, 12] have also been reported, but sometimes with contradictory results.

We chose here to consider and modify EVs with physical methods used for synthetic vectors, and state on their added value in regard to the use of such vectors, for instance liposomes. Considering classic size standards, we chose to focus on small (inferior to 150 nm) and endosomal sourced vesicles i.e. exosomes. We adopted the new guidelines of the EV community [13] and use

the term small EVs, rather than exosomes, as the overlapping in size, similar morphology and variable composition make the distinction of EV type by current purification methods difficult. We used murine mesenchymal stem cells (mMSC) to produce EVs as they produce large quantities of EVs without external stress which can affect EV composition [14, 15]. Those EVs have low immunogenicity [16, 17] and have shown promise in preclinical and clinical studies [18, 19]. MSC have even been described as the only cell type known to have a scalable capacity to mass produce EVs, making it an ideal candidate for production of EVs destined for delivery [16]. We first focused on identifying a robust and reproducible protocol to produce and isolate EVs. We then ensured thorough characterisation of obtained EVs. For this, we used an extensive characterisation panel based on complementary physico-chemical – hydrodynamic diameter and concentration (Nanoparticle Tracking Analysis (NTA)), surface charge (electrophoretic mobility), structure (cryoTEM) – and biological methods – whole protein quantification (microBCA), presence of small EV enriched markers CD81, TSG101, ADAM10 (western blot), qualitative whole protein content (high-throughput comparative proteomics, nano-LC MS/MS), qualitative lipid content (lipidomics), qualitative micro RNA (miRNA) content (transcriptomics). To our knowledge, such characterisation combination is rarely encountered in the field. As the majority of EV research is performed with freshly isolated EVs, which is inconvenient for a rational therapeutic use, we specifically worked on finding optimal storage conditions. In order to obtain with EVs the freedom and ease of use existing with synthetic nanoparticles, we focused on the evaluation of colloidal stability of EVs, rather than only on whole protein content or the presence of specific markers. We next monitored EV internalisation into cells and characterised their uptake pathway using chemical endocytic pathway inhibitors, in comparison to synthetic liposomal systems currently used as a standard. With the specific care of using the same particle number, we evidenced the interest of using EVs instead of liposomes, as shown by increased cell internalisation efficiency. We next evaluated the effect of physical post-production modifications, namely extrusion (50 nm polycarbonate membrane), sonication and freeze-drying, on EV structure, concentration, colloidal behaviour and internalisation ability. Altogether, we obtained reproducible EV suspensions enriched in small EV markers (proteomics), stable to freeze-drying in terms of structure and composition. We are finally convinced that EV could be rationally used as drug delivery systems, especially in regards to their promising interaction with target cells.

## 2. Materials and methods

### 2.1. Materials

Culture media and additives were purchased from Gibco LifeTechologies (USA): Dulbecco's Modified Eagle Medium (DMEM), Foetal Bovine Serum (FBS), penicillin/streptomycin, L-glutamine, trypsin-EDTA, Opti-MEM, Dulbecco's Phosphate-Buffered Saline (DPBS).

Chemicals were purchased from (i) Sigma-aldrich (France): D-trehalose, Bovine Serum Albumin (BSA), Laemmli concentrate sample buffer 2X , Tris-Glycine-SDS buffer 10X, Tris-base, Tween20, Glycine, methanol, Sodium DodecylSulfate (SDS), chloroform, Hank's Balanced Salt Solution (HBSS), cytochalasin D, chlorpromazine, methyl-β-cyclodextrin (MBC), genistein, Hoechst 33342 ; (ii) Thermofisher (France): microBCA kit (23235), DiD (1,1'--dioctadecyl-3,3,3',3'-tetramethylindodicarbocyanine), DiI (1,1'-Dioctadecyl-3,3,3',3'-Tetramethylindocarbocyanine perchlorate), protease inhibitors (32953), PVDF membranes, Lab-Tek chambered coverglass system (8 chambers) ; (iii) Lipoid (Switzerland) : Hydrogenated Soy PhosphatidylCholine (HSPC) and (iv) Avanti (USA): cholesterol.

### 2.2. Cells

Mesenchymal stem cells (mMSC Bl6-GFP, designated as mMSC) were kindly provided by the team of Danièle Noël (IRMB, INSERM U1183, Montpellier), isolated and characterised following protocols previously described [20]. NIH3T3 cells were purchased from ATCC (USA). mMSC and NIH3T3 were cultured in DMEM supplemented with 10% FBS, 2 mM L-glutamine, 100 U/mL penicillin and 100 µg/mL streptomycin, and grown in an incubator in optimal conditions of 37°C and 5% $CO_2$.

### 2.3. Liposome formulation

Liposomes were formulated to match the composition of the commercial standard Doxil® [21, 22]: Hydrogenated Soy Phosphatidylcholine (HSPC) / Cholesterol (56:39, mol:mol). They were synthesized by film-hydration-rehydration method. HSPC and cholesterol were weighed and dissolved in chloroform at 5 mg/mL total concentration. Chloroform was evaporated using a rotary evaporator and the dried film was resuspended in DPBS at 3 mg/mL and stored for hydration at 4°C overnight. The lipid suspension was extruded using a syringe-based hand-held mini-extruder LiposoFast-Basic (Avestin, Canada) (through a 100 nm pore size membrane, 50 times). Size and concentration (particles/mL) were determined by NTA (section 5.1): results are presented in Figure S1.

### 2.4. Separation and concentration of mMSC-derived EVs from cell culture medium

mMSC were cultured to reach 70% confluence. Cells were then washed with DPBS and further cultured in reduced serum medium Opti-MEM for 48h (cell aspect was monitored before and after serum depletion, Figure S2). The medium was collected and centrifuged at 300 g for 10 min at 4°C to eliminate dead cells. The supernatant was centrifuged at 2,000 g for 20 min at 4°C to eliminate cell debris, filtered (through a 0.22 µm membrane) to eliminate large vesicles and stored at 4°C overnight. This medium was then ultra-centrifuged in a 45Ti rotor (Beckman Coulter, USA) with an Optima XPN-80 Ultracentrifuge (Beckman Coulter, USA) at 100,000 g (35,800 rpm) for 110 min at 4°C to pellet small EVs (k factor: 209.6). The supernatant was discarded and EVs were washed with DPBS and centrifuged a second time under the same conditions. All information regarding "Minimal information for studies of extracellular vesicles" (MISEV) 2018 guidelines about EV production [13] are listed in Table S1. The EV pellet was finally resuspended in 1-2 mL of freezing buffer: DPBS, trehalose 25 mM in DPBS or trehalose 25 mM in DPBS supplemented with protease inhibitors. EVs were stored at 4°C, -20°C or -80°C until use. EVs characterised by western blot, lipidomics, proteomics, transcriptomics, modified by physical processes, incubated with cells were previously stored at -80°C in trehalose 25 mM in DPBS with or without protease inhibitors.

### 2.5. Characterisation

#### 2.5.1. Nanoparticle Tracking Analysis (NTA)

Nanoparticle (EV or liposome) suspensions were analysed with a NanoSight NS300 (Malvern Instruments, UK). Suspensions were diluted with particle-free DPBS to obtain a particle concentration in the 1 x $10^7$ - 1 x $10^9$ particles/mL range, as recommended by manufacturer. Measurements were performed with a 405 nm laser. EV suspensions were analysed using the NanoSight NTA 3.2 software following a tailored script: temperature was set at 25°C, syringe pump at 40 AU (arbitrary unit), 3 videos of 60 seconds were recorded. Videos were recorded with a camera level set to 16 and analysed with a detection threshold set to 6.

#### 2.5.2. Dynamic Light Scattering (DLS) and zeta potential

EV suspensions were analysed with a Zetasizer Nano ZS (Malvern Instruments, UK) equipped with a He–Ne laser (wavelength: 632.8 nm) at a temperature of 25°C and a scattering angle of 173° for detection. Size distribution and zeta potential were measured in DPBS.

### 2.5.3. MicroBCA (Bicinchoninic acid)

EV suspensions and cell lysates were diluted with DPBS to reach an absorbance comprised within standard curve range (0-200 µg/mL BSA in DPBS) before analysis by microBCA assay following manufacturer's instructions. Absorbances were read at 562 nm using a Multiskan GO spectrophotometer (N10589, ThermoScientific, USA).

### 2.5.4. Western blotting

Cells were lysed in cell lysis buffer (300 mM NaCl, 50 mM Tris, 0.5% Triton X-100, pH 7.4) supplemented with protease inhibitors. EVs and cell lysates (2.5 µg) were mixed 1:1 with SDS reducing buffer (Laemmli buffer) (or non-reducing equivalent for detection of CD81), heated at 95°C for 5 min and put on ice. Samples were run through 10% polyacrylamide SDS-PAGE (sodium dodecyl sulfate–polyacrylamide gel electrophoresis) gels in Tris-Glycine-SDS buffer. Samples were transferred onto PVDF membranes via semi dry-transfer using a Trans-Blot SD system (BioRad, France) in transfer buffer (48 mM Tris, 39 mM glycine, 20% methanol, 0.0375 % SDS). Membranes were blocked for 1h-1h30 in 3% BSA solution in TBS-T (TBS-Tween 20 0.1%) before overnight incubation at 4°C with primary antibodies: ADAM10 (1:1000, ab1997, Abcam, France), CD81 (1:1000, clone Eat-2, MCA1846GA, BioRad, France), TSG101 (1:1000, 14497-1-AP, ProteinTech, France), beta actin (1:7500, 20536-1-AP, ProteinTech, France). After 3 washes in TBS-T, membranes were incubated for 1h at RT with HRP-conjugated secondary antibodies: goat anti-rabbit IgG H&L (1:5000-1:10000, ab97051, Abcam, France), rabbit anti-armenian hamster IgG H&L (1:10000, ab5745, Abcam, France). Membranes were visualised by chemiluminescence using Immobilon ECL reagents (WBKLS0500, Merck) on a Chemismart 5000 imager (Fisher Bioblock, France).

### 2.5.5. Proteomics

A quantity of 20 µg of proteins were extracted from vesicles by adding LDS buffer (Invitrogen, USA) and subjecting them to a short migration on a denaturing SDS-PAGE gel as previously described [23]. Each batch was analysed in analytical duplicates. Peptides were generated by in-gel trypsin proteolysis and were identified by tandem mass spectrometry. NanoLC-MS/MS experiments were performed on a Q-Exactive HF high resolution tandem mass spectrometer (ThermoFisher, USA) coupled to an UltiMate 3000 LC system (Dionex-LC Packings, France). Peptide samples (2 µL) were loaded and desalted online on a reverse-phase precolumn (C18 PepMap 100 column, LC Packings) and then resolved on a nanoscale C18 PepMapTM 100 capillary column (LC Packings) at a flow rate of 0.3 µL/min with a 60-min gradient from 2.5% to 40% solvent B consisting of 0.1% HCOOH, 80% $CH_3CN/H_2O$ while solvent A was 0.1% HCOOH, 100% $H_2O$. Full-scan mass spectra were measured from m/z 300 to 1800 at 60,000 resolution in data-dependent mode using the TOP20 mode. In this

mode, a scan cycle was initiated with a full scan followed by successive MS/MS scans at 15,000 resolution on the twenty most abundant ions. Interpretation of MS/MS spectra was performed with the MASCOT software (MatrixScience) as previously described [24] against the *Mus musculus* protein sequence database from NCBI with a maximum of two missed cleavages.

**2.5.6. Lipidomics**

*Lipid extraction*

Lipids from EVs corresponding to 200 µg protein (quantified by BCA) were extracted following a protocol adapted from Bligh and Dyer [25] in dichloromethane/methanol (2% acetic acid) / water (2.5 : 2.5 : 2 v/v/v), in the presence of internals standards (ceramide (Cer) d18:1/15:0 16 ng; phosphatidylethanolamine (PE) 12:0/12:0 180 ng ; phosphatidylcholine (PC) 13:0/13:0 16 ng ; sphingomyelin (SM) d18:1/12:0 16 ng ; phosphatidylinositol (PI) 16:0/17:0 30 ng ; phosphatidylserine (PS) 12:0/12:0 156.25 ng, 4 µg of stigmasterol, 4 µg of cholesteryl heptadecanoate and 8 µg of glyceryl trinonadecanoate). The solution was centrifuged at 1,500 rpm for 3 min. The organic phase was collected and dried under nitrogen, then dissolved in 20 µL of ethyl acetate for neutral lipid analysis and then in 50 µL in MeOH for main phospholipids and sphingolipids profiling. The extract was then stored at -20°C prior to analysis.

*Phospholipids, ceramides and sphingolipids profiling*

Main phospholipids and sphingolipids were profiled using an Agilent 1290 UPLC system coupled to a G6460 triple quadrupole spectrometer (Agilent Technologies, USA) and using MassHunter software for data acquisition and analysis. A Kinetex HILIC column (Phenomenex, USA, 50 x 4.6 mm, 2.6 µm) was used for LC separation. Column temperature was controlled at 40°C. The mobile phase A was acetonitrile; and B was 10 mM ammonium formate in water at pH 3.2. The gradient was as follows: from 10% to 30% B in 10 min; 10-12 min, 100% B; and then back to 10% B at 13 min for 1 min re-equilibrium prior to the next injection. The flow rate of mobile phase was 0.3 mL/min and the injection volume was 5 µL. An electrospray source was employed in positive (for Cer, PE, PC and SM analysis) and negative ion mode (for PI and PS analysis). The collision gas was nitrogen. Needle voltage was set at + 4000 V. Several scan modes were used. First, to obtain the naturally different species masses, cell lipid extracts were analysed with a precursor ion scan of 184 m/z, 241 m/z and 264 m/z to PC/SM, PI and Cer respectively; and a neutral loss scan of 141 and 87 to PE and PS respectively. The collision energy optimums for Cer, PE, PC, SM, PI, PS were 25 eV, 20 eV, 30 eV, 25 eV, 45 eV, and 22 eV respectively. The corresponding Selected Reaction Monitoring (SRM) transitions were then used in order to quantify different phospholipid species for each class. Two Multiple Reaction Monitoring (MRM) acquisitions were necessary because of important differences between

PL classes. Data were treated using QqQ Quantitative (vB.05.00) and Qualitative analysis software (vB.04.00).

*Neutral lipid molecular species analysis*

1 µL of the lipid extract was analysed by gas-liquid chromatography on a FOCUS Thermo Electron system using an Zebron-1 Phenomenex fused silica capillary columns (5 m x 0.32 mm i.d, 0.50 µm film thickness) [26]. Oven temperature was programmed from 200°C to 350°C at a rate of 5°C per min and the carrier gas was hydrogen (0.5 bar). The injector and the detector were at 315°C and 345°C respectively.

*Eicosanoids profiling*

For extraction, lipids corresponding to 200 µg (protein, quantified by BCA) of EVs were crushed with a FastPrep ®-24 Instrument (MP Biomedical, USA) in 1 mL of HBSS (Invitrogen, USA). After 2 crush cycles (6.5 m/s, 30 s), homogenates were withdrawn for oxylipins analyses. 300 µL of cold methanol and 5 µL of internal standard (Deuterium labelled compounds) were added. After centrifugation at 900 g for 15 min at 4°C, supernatants were transferred into 2 mL 96-well deep plates and diluted in $H_2O$ to 2 mL. Samples were then submitted to solid phase extraction (SPE) using OASIS HLB 96-well plate (30 mg/well, Waters) pretreated with MeOH (1 mL) and equilibrated with 10% MeOH (1 mL). After sample application, the extraction plate was washed with 10% MeOH (1 mL). After drying under aspiration, lipid mediators were eluted with 1 mL of MeOH. Prior to LC-MS/MS analysis, samples were evaporated under nitrogen gas and reconstituted in 10 µL of MeOH. LC-MS/MS analysis of eicosanoids was performed as described [27]. Briefly, lipid mediators were separated on a ZorBAX SB-C18 column (2.1 mm, 50 mm, 1.8 µm) (Agilent Technologies, USA) using Agilent 1290 Infinity HPLC system (Agilent Technologies, USA) coupled to an ESI-triple quadruple G6460 mass spectrometer (Agilent Technologies, USA). Data were acquired in Multiple Reaction Monitoring (MRM) mode with optimised conditions (ion optics and collision energy). Peak detection, integration and quantitative analysis were done using Mass Hunter Quantitative analysis software (Agilent Technologies, USA) based on calibration lines built with commercially available eicosanoids standards (Cayman Chemicals, USA).

**2.5.7. Transcriptomics (small RNAseq)**

*RNA isolation*

EV pellets (freeze-dried or not) were resuspended in Qiazol lysis buffer and RNA was extracted following RNeasy Micro kit with a DNAse treatment step (Qiagen, Courtaboeuf, France). RNA was then quantified spectrophotometrically (Nanodrop ND-1000, Wilmington DE) and RNA quality was assessed by capillary electrophoresis on an Agilent 2100 Bioanalyzer (Agilent Technologies Inc, Santa Clara, CA).

*Library construction*

Micro RNAs were quantified on a Fragment Analyzer (Agilent) using the smallRNA Analysis kit (DNF-470-0275). Libraries were constructed using the NEXTFLEX Small RNA-seq kit v3 (Perkin Elmer, NOVA-5132-05) following the manufacturer's instructions. Briefly, a 3' adenylated adapter was ligated to the 3' end of 0.2 ng of microRNA and purified to remove excess 3' adapter. A 5' adapter was ligated to the 5' end of the 3' ligated microRNA. The resulting construction was purified to remove excess 5' adapter. 5' and 3' ligated microRNAs underwent un reverse transcription using a M-MuLV reverse Transcriptase and a RT primer complementary to the 3' adapter. Resulting cDNAs were used as a matrix in a 25 cycles PCR using one universal and one barcoded primer. The resulting barcoded library was size selected on a Pippin HT (SAGE SCience) using 3 % agarose cassette (HTG3004) and aiming for a size range between 126 base pairs (bp) and 169 bp. Once size was selected, libraries were verified on a Fragment Analyzer using the High Sensitivity NGS kit (DNF-474-0500) and quantified using the KAPA Library quantification kit (Roche, KK4824). Libraries were equimolarly pooled and sequenced on one lane single read 50 nucleotide on an Hiseq2500 (Illumina) using the rapid cluster and SBS kit v2.

*Sequencing and analysis*

Image analyses and base calling were performed using the HiSeq Control Software and Real-Time Analysis component (Illumina). Demultiplexing was performed using Illumina's conversion software (bcl2fastq 2.20). The quality of the raw data was assessed using FastQC from the Babraham Institute and the Illumina software SAV (Sequencing Analysis Viewer). The raw reads were trimmed using Cutadapt (version 2.3) [28] to remove the sequencing adapter (TGGAATTCTCGGGTGCCAAGG) at the 3'-end. Additionally, 4 bases were also trimmed from the 5'-end and 3'-end of the reads as indicated in the manual of NEXTflex Small RNA-Seq Kit v3 from Bioo Scientific. MicroRNA analysis was performed with miARma v1.7.3 pipeline [29]. In this pipeline, alignment was performed with Bowtie v1.1.2 (--best --strata -M 1 --chunkmbs 1000 options) to the mouse genome (GRCm38). The microRNA annotation was retrieved from miRBase (v22). Counting of reads aligned to a miRNA was performed with Featurecounts v1.5.0-p1 (-s 1 -t miRNA -g Name options). Before statistical analysis, genes with less than 15 reads (cumulating all the analysed samples) were filtered out. Differentially expressed miRNA were identified using three Bioconductor [30] packages: edgeR 3.20.9 [31], DESeq 1.30.0 [32] and DESeq2 1.18.1 [33]. Data were normalised using the Relative Log Expression (RLE) [33] normalisation factors for edgeR package and the default method for other packages. miRNA with adjusted p-value less than 5% (according to the FDR method from Benjamini-Hochberg) were declared differentially expressed.

### 2.5.8. CryoTEM (transmission electron cryomicroscopy)

3 µL of undiluted EV suspension were applied to glow discharged Lacey grid (Ted Pella Inc., USA), blotted for 1s and then flash frozen in liquid ethane using a CP3 cryo-plunge (Gatan Inc., USA). Before freezing, the humidity rate was stabilised at about 95%. CryoTEM was carried out on a JEOL (JEOL (Europe) SAS) 2200FS FEG operating at 200 kV under low-dose conditions (total dose of 20 electrons/Å2) in zero-energy-loss mode with a slit width of 20 eV. Images were taken with a slow-scan CCD 4k x 4k camera (Gatan Inc., USA) at a nominal magnification of 50,000 x corresponding to a calibrated magnification of 45,591 x with defocus ranging from 1.8 to 2.2 µm.

## 2.6. EV post-production modifications

### 2.6.1. Extrusion

EV suspensions were analysed by NTA and diluted to 2-3 x $10^9$ particles/mL. Diluted suspensions were extruded at RT using a syringe-based hand-held mini-extruder LiposoFast-Basic (Avestin, Canada) through a 100 nm pore size polycarbonate membrane 40 times, through a 50 nm pore size membrane 40 times. The resulting suspensions were analysed by NTA.

### 2.6.2. Sonication

EV suspensions were analysed by NTA and diluted to 2.5-5 x $10^9$ particles/mL. Suspensions were sonicated using a sonication probe Digital Sonifier 250 (Branson Ultrasonics Corporation, USA) with a Microtip 64-247A for 6 cycles of 80 seconds on/off (duty cycle 60%) with 20% amplitude and 2 min of cooling period between each cycle, on ice. The resulting suspensions were analysed by NTA.

### 2.6.3. Freeze-drying

To optimise freeze-drying protocol, different initial concentrations of EVs (<1; 1-2; > 2 x $10^{10}$ EVs/ml), initial freezing volumes (<150 µL or > 150 µL), and the presence or absence of protease inhibitors (-PI, +PI) were evaluated. EV suspensions were diluted to 0.25-5 x $10^{10}$ particles/mL in DPBS supplemented with trehalose 25 mM and frozen at -80°C, freeze-dried overnight (Heto PowerDry LL 3000 Freeze Dryer, ThermoScientific, USA) and resuspended in milliQ water. The resulting suspensions were then left to hydrate at 4°C for 1h and analysed by NTA.

## 2.7. Nanoparticle internalisation by microscopy

EV or liposomal suspensions (1 x $10^{10}$ particles/mL) were stained with DiI (1 µM). No significant nanovesicle aggregation was observed by DLS. DiI-labelled EVs or liposomes (9 µL, 9 x $10^7$ particles) were incubated for 30min-2h30 at 37°C with mMSC or NIH3T3 at 80% confluence in 96-well plates in

complete culture medium. Cells were then washed (DPBS, 2 min, 3 times), complete culture medium was added and cells were observed with an EVOS microscope AMF4300 (Life Technologies, USA). Transmitted and RFP (for DiI fluorescence) channels were visualised, and merged images were generated using the EVOS microscope interface. For confocal microscopy experiments, EV or liposomal suspensions (1 x $10^{10}$ particles/mL) were similarly stained with DiD (1 µM), and DiD-labelled EVs or liposomes (20 µL, 2 x $10^{8}$ particles) were incubated for 2h at 37°C with NIH3T3 at 80% confluence in Lab-Tek 8-chamber systems in complete culture medium. Cells were then washed with culture medium and cells were incubated with culture medium with Hoechst nuclear stain (10 µg/mL) for 40 min. Cells were finally washed (culture medium without phenol red, twice), complete culture medium without phenol red was added and cells were observed with a spinning disk (Dragonfly, Andor, Oxford Instruments, UK) which allowed fast 3D imaging. Lasers were used as excitation sources (405 nm for Hoechst nuclei staining and 640 nm for DiI). A 100x, NA 1.45 Nikon objective was used for maximum resolution. The fluorescence signal was detected on an ultra sensitive EMCCD camera (iXon Life 888, Andor). For the z-stacks a z step of 300 nm was used. Transmitted, Hoechst (nuclei) fluorescence and DiD (vesicles) fluorescence channels were visualised, and merged images were generated using Image J software.

**2.8. Nanovesicle internalisation by flow cytometry**

Nanovesicles (EV or liposomal suspensions) (1 x $10^{9}$ particles/mL) were stained with DiD (0.1 µM) by co-incubation 1h at 37°C. No significant nanovesicle aggregation was observed by DLS. DiD-labelled EVs or liposomes (100 µL, 1 x $10^{8}$ particles) were incubated for 2h at 37°C with mMSC or NIH3T3 at 70-80% confluence in 12-well plates in complete culture medium. Cells were collected using trypsin-EDTA, washed twice with DPBS, centrifuged (1,800 rpm, 5 min, 4°C) and finally resuspended in HBSS without $Ca^{2+}$, $Mg^{2+}$ before analysis by flow cytometry on a BD Accuri C6 (BD Biosciences, USA) (20,000 events were counted for each sample). Fluorescence mean values (in the FL4 channel where DiD fluorescence was observed) were normalised to that of cells incubated with DiD-labelled EVs. When endocytic pathways inhibitors were used, cells were pre-incubated with chemical inhibitors for 1h prior to the addition of labelled vesicles. The inhibitors were used at the following final concentrations: 5 µg/mL chlorpromazine, 5 µg/mL cytochalasin D, 3 mg/mL methyl-β-cyclodextrin, 200 µM genistein, as these concentrations were evaluated and do not induce cell cytotoxicity [20]. Modified EVs (extruded, sonicated, freeze-dried) were stained following the protocol described above (1 x $10^{9}$ particles/mL, 0.1 µM DiD, 1h at 37°C). DiD-labelled modified EVs were used at the same concentration (100 µL, 1 x $10^{8}$ particles) and were incubated for 2h at 37°C with mMSC or NIH3T3.

### 2.9. Statistical analysis

Statistical tests were performed using OriginPro software 8.5 (OriginLab, USA). One-sample t-tests were performed when comparing an average to a theoretical value (percentages to 100%); two-sample t-tests when comparing two averages of unpaired values; pair-sample sample t-tests when comparing two averages of paired values (for instance, EV average mode or mean before and after modification). Differences were considered statistically significant when p values were inferior to 0.05. Results were indicated on graphs as follows: * : $p<0.05$, ** : $p<0.01$, *** : $p<0.001$; *, ** or *** above an error bar without any other precision means the average was compared to a theoretical percentage of 100%.

## 3. Results

### 3.1. Characterisation of mMSC-derived EVs

After separation and concentration of EVs from serum free culture media, EV suspensions were characterised using a panel of physico-chemical and biological techniques. A typical batch of EVs yielded 9.7 ± 3.5 x $10^8$ EVs (n=20) per million producing cells (Figure 1A), from an average of 85 million cells. This value seemed to correlate with protein quantity per million producing cells, as the protein quantity per EVs varied little between batches with an average amount of 22.7 ± 5.7 µg / $10^{10}$ EVs (Figure 1A). EVs were 94.4 ± 10.3 nm (n=20) regarding majority population (mode) identified by NTA (Figures 1A&B). EVs exposed a slightly negative surface charge of -15 ± 2 mV (n=4) (Figure 1A). As observed by cryoTEM imaging (n=5) (Figure 1D), vesicles were spherical and their diameter averaged 100 nm with a visible lipid bilayer formed by two parallel dark lines corresponding to the two leaflets.

EVs were shown to express ADAM10, TSG101 and CD81, proteins generally associated with small EVs expressed by endosomal sourced vesicles (exosomes) [34] while cell lysates did not (western blot analysis (n=4); Figure 1C). Full EV protein content was identified by shotgun proteomics taking into account three experimental replicates (Figures 2, S3). The high performances of the tandem mass spectrometer used for this identification resulted in an exhaustive catalogue of proteins with a total of 1,241 proteins validated with at least two different peptides. The abundances of these proteins were evaluated based on their spectral counts. To allow an easier reading of proteomics results, among the 1,241 proteins identified with 2 peptides (Figure S3, sheet 2), we added a colour identification of proteins as a function of their belonging to categories described in Théry *et al.*, 2018 (MISEV 2018, Table 3)[13] : (i) category 1 in blue (transmembrane or GPI-anchored

proteins associated to plasma membrane and/or endosomes), (ii) category 2 in green (cytosolic proteins recovered in EVs), (iii) category 3 in red (major components of non-EV co-isolated structures), (iv) category 4 in orange (transmembrane, lipid bound and soluble proteins associated to other intracellular compartments than PM/endosomes), (v) category 5 in purple (secreted proteins recovered with EVs). Functional proteins were coloured in bright colours while precursors were coloured in pale colours. Among the 1,241 proteins identified with 2 peptides, we categorised 185 proteins in the previously evocated categories. Figure 2A presents some of the identified proteins, as well as some we did not detect. Amidst these 185 proteins, 2% belong to category 1, and 72% to category 2, two categories which could be related to EV markers. 16% belong to category 3, while 10 % in category 4 and only one category 5 protein were detected (precursors or pre-proteins were identified) (Figure 2B). Furthermore, this category 5 protein was osteoclast-stimulating factor 1, which is consistent with mMSC being the EV producing cells (Figure S3, sheet 2). Major components of non-EV co-isolated structures (i.e. apolipoproteins, albumin; category 3) were not identified following our identification criteria (at least 2 peptides). Nevertheless, ribosomal proteins, frequently reported as co-isolated with EVs, were found (52 proteins of the total 1,241 identified) representing 6.4% of the total signal (Figure S3, sheet 2). None of the classically detected mitochondria proteins were detected (Inner Membrane Mitochondria protein (IMMT), or TOMM20) whereas 11 mitochondria associated precursor proteins were identified. No endoplasmic reticulum or Golgi associated proteins (such as Endoplasmic reticulum chaperone BiP (HSPA5), Golgi subfamily A member 2 GM 130 (GOLGA2)) as well as no autophagosomes markers (Atg9a) were detected. Cytokeratin, a main component of cytoskeleton, was also absent in the 1,241 proteins identified with 2 peptides. We did also observe mitochondrial histones (especially histone H4) and histone associated proteins, despite these proteins being reported to be mainly associated to large EVs rather than to small ones [35]. Finally, as MSC are well known for their secretory properties, we particularly looked at secreted proteins. Interestingly, none of the secreted proteins we searched for (VEGF, TGF, IFN, FGF, PEDGF, EGF, HGF, MMP1, TIMP2 or interleukins (IL6)) were recovered in EVs. None of the classic membrane markers of mMSC (CD73, CD90, CD105, CD106, sca-1) were detected in EVs. In contrast, adhesion proteins, as well as tetraspanins, involved in cellular docking and internalisation [36-38], were present in all three EV samples. Importantly, we noted EV protein content was mostly conserved among the three batches tested, with (i) 927 proteins out of the 1,241 present in all three batches (75%), and 90% present in at least two out of three batches (Figure 2C) and (ii) total spectral counts of the 927 proteins common to the three batches (taking into account the biological triplicates and the technical duplicates) representing 95% of the total spectral counts measured, thus corresponding by far to the most abundant proteins (Figure S3, sheet 5).

In parallel to protein content analysis, we decided to analyse lipid content with the goal of evaluating (i) if EV lipid composition could explain increased interaction with cells (see section 3.4.1 and discussion section) and (ii) if lipid composition could explain EV behaviour in regards to future physical constraints we planned to apply. Lipidomics analysis (n=3) revealed the presence of numerous classes of lipids: ceramides (Cer), sphingomyelins (SM), phosphatidylcholines (PC), phosphatidylethanolamines (PE), phosphatidylserines (PS), phosphatidylinositols (PI) (Figure 3), eicosanoids and cholesterol (15.8 ± 3.6 relative abundance/mg of protein) (Figure S4). No other neutral lipids (cholesterol esters, triacylglycerols) were detected. We observed remarkable consistency amongst the three EV batches, with limited standard errors. Ceramides (Figure 3A) were mostly short chain mono-unsaturated Cer d18:1 / 16:0 (63 ± 3 % of the relative quantification of this lipid class); the same tendency was observed in sphingomyelins (Figure 3B), with a majority of SM 18:1 / 16:0 (65 ± 1 %). For phosphatidylserines, phosphatidylcholines and phosphatidylethanolamines (Figures 3C,D,E), the majority species within each class were mono-unsaturated: PS 36:1 (30 ± 0.5 % of the relative quantification of this lipid class), PC 34:1 (27 ± 1 %) and PE 36:1 (22 ± 1 %) respectively. As for phosphatidylinositols (Figure 3F), the majority species are PI 38:3 (23 ± 0.1 %) and PI 38:4 (24 ± 1 %), both long chain polyunsaturated lipids. With the extraction method used, two eicosanoids were detected: 13-HODE (44.9 ± 20.5 pg/µg of protein, n=3) and 9-HODE (6.0 ± 3.5 pg/µg of protein, n=3) (Figure S4).

Finally, EV miRNA content was analysed by transcriptomics (Figures S5&6). Considering miRNAs detected with at least 5 reads in one of the two unmodified EV samples (in terms of normalised counts), 339 miRNAs were identified (Figure S5, sheet 3). Similar to what was observed in proteomics analysis, miRNA content was highly conserved among the two batches tested, with: (i) 237 miRNAs out of the 339 present in both batches (70%) (Figure S6A), (ii) 17 out of the 20 top miRNAs found in one batch (ranked by decreasing normalised count) were found in the top 20 of the other batch (Figure S6B).

### 3.2. Determination of optimal EV storage conditions

Using EVs in therapy requires either the use of fresh EVs or optimal EV conservation before use. We explored solutions to store EVs before modifications and use, and evaluated the influence of these storage conditions on EV concentration by NTA (in contrast with classic whole protein content or specific marker tracking). We first monitored the effect of freeze-thaw cycles (from -20°C or -80°C to room temperature) on EV concentration (NTA) over 28 days (freezing in DPBS, a classic buffer used to store EVs): we kept aliquots that were thawed only on the day of the measurement and others that were thawed on the first measurement day, then frozen again until the next measurement, and

so on (Figure S7). We identified a marked decrease in concentration: on day 28, samples frozen and thawed only once had a concentration 32% that of concentration on day of isolation (D0) whereas samples that had been through 7 freeze-thaw cycles were down to 13 %. In cryoTEM imaging, we observed the formation of multivesicular, concentric particles (Figure 4A), at a nearly 1:1 ratio with unilamellar vesicles (45%/55% multivesicular / unilamellar).

To identify the best conditions for storage, EVs were stored at various temperatures: 4°C (Figure 4B), -20°C (Figure 4C) and -80°C (Figure 4D) in three different storage buffers: (i) DPBS, (ii) trehalose 25 mM (cryoprotectant) (TRE) and (iii) trehalose 25 mM complemented with protease inhibitors (PI) (TRE-PI). EV suspensions were aliquoted on the final day of isolation (day 0, D0), and the concentration on day X (DX) was expressed as a percentage of the concentration measured on D0. At 4°C, when stored in DPBS, a significant decrease was observed on D3-5 with 68 ± 10% of EV conservation (EVs still detected) (Figure 4B). No significant further decrease was observed thereafter, as on D7 and D13-17 EV concentration remained in this range (62 ± 19% and 67 ± 12% respectively). The uses of TRE or TRE-PI led to a decrease in EV concentration but in a more acceptable range on D13-17 (91 ± 4% and 90 ± 17% respectively). At 20°C, when stored in DPBS, a significant decrease in concentration was observed starting from D1 (79 ± 15%) (Figure 4C). A continuous decrease was thereafter observed over time, from D3-5 (67 ± 17%) to D13-17 (48 ± 12%). Still at this temperature, the use of TRE-PI led to significantly less important decrease with concentration reaching 90 ± 11% on D1, 86 ± 16% on D3-5, 87 ± 12% on D7, and 89 ± 7% on D13-17 compared to D0 (100%). In contrast, the use of TRE without PI did not lead to significant stability improvement compared to DPBS, on D13-17 the final concentration was 69 ± 14%. Regarding -80°C storage, DPBS still led to concentration decrease, with values falling to 77 ± 10% on D1 (Figure 4D). At this temperature, in contrast with -20°C, the addition of TRE to DPBS increased the overall stability and led to EV concentrations of 93 ± 13% on D7 and 88 ± 14% on D13-17, significantly increased ($p<0.01$) compared to DPBS alone on D13-17 (51 ± 12%). The buffer leading to the best concentration values remained DPBS supplemented with TRE and PI, with values of 89 ± 22% on D1 and still at 89 ± 10% on D13-17. Given these results, we identified freezing EV suspensions in trehalose 25 mM with or without PI at -80°C as the optimal EV storage conditions. CryoTEM images confirmed these protocols did not alter EV structure (Figures 4E&F).

With the goal of long-term storage, we have considered freeze-drying. EVs were frozen at -80°C in trehalose 25 mM and dried overnight. We examined the influence of the following parameters on EV concentration: addition of PI to trehalose when freezing, starting EV concentration, freezing volume ($n\geq6$) (Figure 5A). The addition of PI tended to increase EV conservation percentages, from 59 ± 24 % to 71 ± 16 %. Freezing in a volume superior to 150 µL resulted in a significantly higher conservation percentage of 70 ± 18 % compared to 36 ± 12 % when

the volume was inferior to 150 µL ($p<0.001$). We also observed a significantly higher conservation percentage when the starting concentration was under 1 x $10^{10}$ particles/mL (67 ± 20 %, $p<0.05$) or between 1 and 2 x $10^{10}$ particles/mL (72 ± 18 %, $p<0.01$) compared to over 2 x $10^{10}$ particles/mL (44 ± 18 %). Overall, we identified that freezing in trehalose with PI at a concentration comprised between 1 and 2 x $10^{10}$ particles/mL in a volume superior to 150 µL were optimal freeze-drying conditions, yielding a 77 ± 12 % recovery (n=4). Furthermore, freeze-dried EVs were analysed by proteomics (Figure S3): 93% of the proteins detected in all three unmodified EV batches were found in freeze-dried EVs (Figure 5B), including CD9, 63, 81, ADAM10, TSG101, syntenin-1, Alix (Figure S3). In terms of spectral counts, total spectral counts of the 862 proteins common to unmodified EVs and freeze-dried represented 95% of total spectral counts of the 1,241 proteins identified. A comparison of the three unmodified EV batches and freeze-dried EVs was performed with the ACfold test proposed for proteomics data comparative analysis [39]. Only 3% of proteins were flagged as statistically differing between unmodified EVs and freeze-dried EVs when a fold change of 1.5 and p value of 0.05 were selected (Figure S3, sheet 6). Overall, proteomics analysis indicated conservation of protein content following freeze-drying. Importantly, proteins known for their involvement in internalisation processes (adhesion molecules, tetraspanins [38]) were preserved after freeze drying (Figure S3, sheet 6). Out of the 65 proteins common to unmodified EV batches which were absent in freeze-dried EVs (Figure 5B), only one (an integrin precursor) belonged to MISEV categories 1 and 2 [13], i.e. small EV protein categories (Figure S3, sheet 5). Additionally, freeze-dried EVs were also analysed by transcriptomics (Figures 5C, S5): statistical analysis did not evidence statistical difference between unmodified EVs (n=2) and freeze-dried EVs (n=3) (DESeq2, $p<0.05$) (Figure 5C and S5, sheet 5). No statistical difference was found using other Bioconductor packages DESeq (Figure S5, sheet 6) and edgeR (Figure S5, sheet 7). These results indicated conservation of miRNA content following freeze-drying.

### 3.3. Evaluation of the impact of physical modifications on EV integrity

EVs were modified by one of the three following physical processes: extrusion through a 50 nm polycarbonate membrane, sonication and freeze-drying. Vesicles were characterised before and after the processes by NTA (Figures 6A&B) and cryoTEM (Figure 6C), to assess the potential impact on EV integrity, structure, and evaluate the loss in EV concentration following the process. NTA results are described regarding mode (diameter of the major population), mean diameter, standard deviation (SD) and concentration (as a percentage of EV concentration before modification) (Figure 6A).

Extrusion reduced the mode and mean of EV suspensions by respectively 21 ± 3 nm ($p<0.01$) and 27 ± 17 nm ($p<0.05$) (n=4), as well as SD from 41 ± 3 nm to 34 ± 19 nm (n=4) (Figure 6A), and resulted in a narrower size distribution (Figure 6B). Concentration tended to increase on average (116 ± 40 % of the concentration before extrusion) (Figure 6A), and cryoTEM imaging revealed EV structure was not impacted, but confirmed EV size reduction, as most vesicles were smaller than 100 nm diameter (Figure 6C).

Sonication significantly reduced EV suspension mode, mean and SD by respectively 14 ± 3 nm ($p<0.05$), 19 ± 4 nm ($p<0.05$) and 11 ± 2 nm ($p<0.01$) (n=3). It also significantly reduced concentration by 34 ± 13 % (n=3) ($p<0.05$) when compared to the concentration before process (Figure 6A). CryoTEM imaging revealed some structural modification of sonicated EVs, as most vesicles were non-spherical and/or had a punctured membrane (Figure 6C).

Freeze drying was investigated with two main goals: (i) to identify a long-term storage solution, and (ii) to produce a dried EV film which could then be rehydrated to load drugs. We present here the results obtained with the optimal conditions we identified and previously described in section 3.2: EV suspensions were frozen in trehalose 25 mM with PI, at a concentration of 1-2 x $10^{10}$ particles/mL, in a volume superior to 150 µL (Figure 5B). Freeze-drying slightly increased the mean (by 14 ± 6 nm, $p<0.05$) and SD (by 13 ± 1 nm, $p<0.001$) of EV suspensions (n=4) (Figure 6A) but EV distribution profile remained mostly unchanged (Figure 6B). EV concentration was reduced by 23 ± 12 % (n=4) ($p<0.05$ when compared to 100%). CryoTEM imaging revealed that EV structure was not impacted as vesicles remained round with double membranes (Figure 6C) as observed before freeze-drying (Figure 1D).

### 3.4. Biological activity – Cell internalisation

#### 3.4.1. Internalisation and endocytic route differences between HSPC/Chol liposomes and EVs

EV internalisation was assessed in two cell types, producing mMSC and foreign cells NIH3T3, to evaluate if a tropism was encountered. EV internalisation was compared to synthetic reference vectors. We chose to use HSPC/Cholesterol (mol:mol 56:39) liposomes representative of the commercial standard Doxil® formulation [21], averaging a size of 123.7 ± 14.3 nm (Figure S1). The same number (9 x $10^7$ for 20,000 cells) of DiI stained nanoparticles were incubated with mMSC (Figure S8) or NIH3T3 (Figure S9) and cells were observed by fluorescent microscopy (epifluorescence (Figures S8&9) and confocal (Figure 7A)). Confocal microscopy images (Figure 7A) showed vesicles were in the same focal plan as the nucleus, evidencing they are localised inside the cell (as opposed to on the surface). Epifluorescence images (Figures S8&9) evidenced that both EVs and liposomes

were internalised to a growing extent over time in mMSC and NIH3T3. In both cell types, EVs seemed to be internalised to a greater extent than liposomes at all time points.

We then quantified this observation by flow cytometry. Cells were treated with DiD stained EVs and liposomes at the same nanoparticle number (1 x $10^8$ for 200,000 cells). After 2h of incubation, cells were analysed. Fluorescence values obtained by flow cytometry were normalised to the mean fluorescence value obtained with cells incubated with labelled EVs (represented as 100%). Liposome internalisation represented 38 ± 22 % and 39 ± 28 % in mMSC and NIH3T3 respectively compared to 100% for EVs (Figure 7B). EVs were therefore internalised to a significantly greater extent than their liposomal counterparts in both cell types.

We next aimed to identify the internalisation pathway used by EVs and liposomes to be internalised into target cells. To this end, cells were pre-incubated with chemical inhibitors of endocytic routes. Cytochalasin D, which depolymerises actin and consequently affects most endocytic processes, was used as a general endocytosis inhibitor. Chlorpromazine, a cationic molecule known to prevent the formation of clathrin-covered pits, was used as an inhibitor of clathrin-dependent endocytosis. Methyl-β-cyclodextrin (MBC), a cyclic oligomer which "extracts" cholesterol from plasma membranes, was used as an inhibitor of cholesterol-dependent endocytic processes. Finally, genistein is a tyrosin-kinase inhibitor which induces a degradation of the actin network in plasma membranes and prevents dynamin II recruitment. These two processes are known for their role in caveolae-dependent endocytosis: genistein was therefore used to inhibit caveolae-dependent endocytosis [40-42]. Cell fluorescence was normalised to the condition of cells incubated with EVs or liposomes without inhibitors (expressed as 100%). Internalisation profiles were similar for mMSC and NIH3T3 (Figure 7C). In mMSC, EV internalisation was decreased in the presence of cytochalasin D (to 33 ± 3 %), slightly decreased in the presence of chlorpromazine (62 ± 5 %), whereas the presence of MBC or genistein led to internalisation levels of 25 ± 5 % and 27 ± 3 %, respectively ($n=4$, $p<0.001$). These results suggest EVs are mainly internalised through a pathway involving caveolae and cholesterol. In mMSC, surprisingly, whereas liposome internalisation was decreased in similar ways in the presence of cytochalasin D, chlorpromazine and genistein (to 38 ± 16 %, 65 ± 7 % and 8 ± 6 % respectively, $p<0.01$), it was greatly increased (186 ± 44 %, $n=4$, $p<0.05$) in the presence of MBC. These data suggest liposomes were internalised through a different pathway than EVs, involving caveolae but not cholesterol. The results obtained in NIH3T3 were similar, suggesting EVs and liposomes were internalised in these cells the same way they are in mMSC. Generally, we noted standard deviations were considerably higher for liposomes than for EVs (Figure 7C).

### 3.4.2. Evaluation of the impact of physical modifications on internalisation

Importantly, we assessed if EV biological properties were maintained after physical processes by evaluating their effect on EV internalisation in mMSC and NIH3T3. For this, EVs, modified or not, were labelled and incubated with cells (same particle number). As previously, we took particular care in monitoring EV aggregation by DLS before use. Internalisation, resulting in cell fluorescence, was normalised to the condition of cells incubated with labelled unmodified EVs (expressed as 100%) (Figure 8). Extrusion and freeze-drying did not significantly impact EV internalisation in mMSC and NIH3T3 (n=3) (Figure 8). For sonicated EVs, internalisation was significantly increased in mMSC: internalisation increased to 205 ± 36 % (n=3, $p<0.05$). In NIH3T3, the increase in internalisation was not statistically significant: internalisation rose to 152 ± 36 % following sonication compared to 117 ± 33 % following freeze-drying and a minor drop to 92 ± 30 % following extrusion (Figure 8). Furthermore, extrusion, sonication and freeze-drying did not change the effect of previously mentioned endocytic inhibitors on EV internalisation (Figure S11).

## 4. Discussion

While EVs have been explored as potential delivery systems over the past two decades, there is still a need to develop reproducible handling methods coherent with a therapeutic use. In this work, we aimed at (i) finding adequate protocols of storage, (ii) establishing the interest of EVs vs. commercial standard nanoparticles and (iii) evaluating the effect of physical modifications on EV physico-chemical and biological properties.

Taking into account differences in production/enrichment protocols, and as the EV field is explored by more and more teams, there is a growing need for exhaustive EV characterisation to be able to compare studies [4, 43]. We therefore characterised EVs with a panel of physico-chemical (NTA, surface charge, cryoTEM) and biochemical techniques (BCA, western blot, proteomics, lipidomics) (Figures 1-3). EV size was comparable to that of liposomal commercial standards we synthesized by lipid film hydration: 94.4 ± 10.3 nm (n=20) for EVs (Figure 1) vs. 123.7 ± 14.3 nm (n=3) for liposomes (Figure S1). Surprisingly, the standard deviation was smaller for EVs whereas this average was performed on 20 batches vs. 3 for liposomes. Focusing on production time and yield, EV production can be performed in 3 days, including two days of cell incubation followed by a “human day of work” for differential ultracentrifugation. Liposome production required roughly the same human manipulation time including lipids weighing, dissolution in solvent, lipid film formation, rehydration overnight, lipid resuspension in aqueous buffer and extrusion. The duration of the

process could be comparable to obtain 5.4 ± 2.7 x$10^{11}$ liposomes/mL (Figure S1) and 8.4 ± 4.2 x$10^{10}$ EVs/mL: the difference is therefore minimal, even if the process we use for purification, as a proof of concept, is known to be time consuming. Several teams published or currently work on less time-consuming protocols that could be investigated in the future to further improve this yield [13].

Proteomics studies allowed the identification of a large catalogue including 1,253 proteins (Figures 2A, S3) and among these, proteins known to be been enriched in exosomes derived from MSC and other cell sources, such as ADAM10, TSG101 and tetraspanins CD81, C9 and CD63 [14, 16, 34, 44-46]. Remarkably, 93 of the top 100 proteins most often encountered in EVs (Vesiclepedia [47]) were identified, which matches previous findings on human MSC-derived EVs [46]. Lipidomics results highlighted the presence of several classes of lipids which have been reported to be enriched in exosomes (Figure 3) [48-56]. Notably, ceramides, implicated in ESCRT-independent exosomes biogenesis, were identified (Figure 3A) [50, 56]. Transcriptomics analysis revealed the presence of several miRNAs previously reported to be present in MSC-derived EVs (Figures S5, sheet 4). They have been described as involved in: (i) MSC differentiation (miR-10a [57], miR-22 [58]), migration (miR-10b [59]) or immune modulatory function (miR-143 [60]) [61]; (ii) cancer growth inhibition (miR-146 [62, 63], miR-16 [64, 65]); (iii) cardioprotection (miR-223 [66], miR-24 and miR-29 [67], miR-22 [68], miR-221 [69], miR-132 [70]). To summarize, even if we know that differential ultrafiltration is an EV enrichment method which leads to intermediate recovery and intermediate specificity [71], the purity of the obtained vesicles seems to reach the criteria of MISEV 2018 as well as our specifications. Indeed, by (i) producing EVs without serum, (ii) performing 0.2 µm filtration and (iii) washing EV pellet with PBS, we managed to obtain nanosized EVs without significant protein contamination (Figures 1-2, S3).

To consider a realistic use of EVs, either for a therapeutic application or as biomarkers, a crucial point is to find optimal storage conditions, as the use of fresh EVs is not a convenient practice. H22 tumour-derived EVs were reported to be unaffected by sunlight exposure, acidic or alkaline conditions, shaking and temperature (RT and 37°C) [72]. However, these results can be questioned as EVs were counted by flow cytometry through fixation on 3 µm latex beads, using an indirect gating strategy. Others teams focused on protein and RNA content [73] or specific markers [74] and showed EVs were more stable at -80°C than at RT [73] or 4°C [74]. These often divergent results could be due to differences in EV production protocols (producing cells, medium, time), in purification protocols, as well as in the readout used to monitor EV stability. If EVs are aggregated, as it has often been reported, or if they are undergoing membrane remodelling, this cannot be detected by performing a protein dosage or a western blot revealing only specific biomarkers. This is why we elected to use tools often used to characterise synthetic vectors, and particularly control aggregation state by controlling hydrodynamic diameter, concentration (NTA) and EV structure (cryoTEM). We evidenced

that using a classic DPBS buffer was not pertinent for mMSC-derived EV storage, regardless of the temperature. We then showed the pertinence of using trehalose (non-reducing disaccharide) (TRE) as it allowed improved dispersion and seemed to protect EVs during freezing especially when stored at -80°C (less than 10% concentration decrease). These results confirmed those of Bosch *et al.* [75] which evidenced an increase in the number of individual particles per microgram of protein of pancreatic beta-cell derived EVs using PBS supplemented with 25 mM TRE. The addition of a cocktail of protease inhibitors (PI) seemed to slightly improve EV conservation although such variations were not significant compared to TRE (Figure 4D). The choice to use or not this type of additive could be left to the discretion of the user. Even though such storage conditions were satisfactory, freeze-drying could be a convenient way to store EVs: it would for instance, avoid any risk of thawing and degradation during shipping. After evaluating several parameters influencing this process (concentration, volume, presence of PI), we identified optimal freeze-drying conditions which allowed a 77 ± 12 % recovery of EVs (Figure 6A). Freeze-drying of EVs has been the subject of very few studies so far [19, 76, 77], as well as one patent (US2016/0158291 A1), with little to no information on the concentration loss after this process. Notably, unlike Frank *et al*. [19] who reported an average size increase of 40 nm when freeze-drying human MSC derived EVs, we noticed very little change in diameter (Figure 6A) (from 99 ± 13 nm to 101 ± 11 nm), distribution profile (Figure 6B), structure (Figure 6C), protein content (Figures 5B, S3) and miRNA content (Figures 5C, S5).

Since we aim at using EVs as alternative drug delivery systems, we evaluated their interest in terms of cell internalisation compared to synthetic commercial standard liposomes. We evidenced that mMSC-derived EVs were internalised to a much greater extent than liposomes (Figures 7A&B, S6, S7), as previously reported [2, 11, 12]. The composition of these two systems could explain this difference. Study of EV lipid content highlighted the presence of cholesterol, frequently used to stabilise liposomes and improve intracellular delivery [78]. The presence of several mono-unsaturated lipids (Figure 3), reported to play a critical role in intracellular bilayer destabilisation and subsequent cell internalisation [78, 79] could be another explanation to increased EV internalisation. Nevertheless, cholesterol and HSPC are also present in the liposomes we used as a control, whereas internalisation levels were much lower. The major difference is the presence of proteins in EV composition. Indeed, adhesion proteins, as well as tetraspanins, known to play a role in cell interaction [36, 37], were detected. We also aimed to identify if internalisation differences could be explained by the way EVs and liposomes enter cells. Although there is no consensus on EV uptake, there is more evidence for exosomal uptake through endocytosis than for direct fusion [5, 80]. However, the exact endocytic process involved is undetermined; it may depend on the cell type, the type of vesicles isolated, or occur as a combination of the following processes: clathrin-dependent

endocytosis, caveole-dependent endocytosis, lipid-raft mediated endocytosis, macropinocytosis and in some cases, phagocytosis [5, 80]. Regarding the effect of endocytic inhibitors, cytochalasin D did reduce internalisation by 60% on average (Figure 7C) which indicates that endocytosis is indeed primarily involved in the interaction of EVs and liposomes with cells. This is in accordance with several other studies which showed cytochalasin D greatly reduced but not completely eliminated EV uptake [45, 80-83]. Furthermore, internalisation at 4°C was negligible, establishing EV (and liposome) uptake to be an energy-dependent process (Figure S10). Our results seem to propose caveolae and cholesterol-dependent pathway as the endocytic process most encountered for mMSC-derived EVs (Figure 7C). Caveolae are membrane domains which are rich in cholesterol, which EVs could bind through sphingolipids such as sphingomyelin, present in EVs we isolated (Figure 3B) [84]. In contrast, liposome internalisation seemed to depend on caveolae but not on cholesterol (Figure 7C). However, for both EVs and liposomes, there was no unique inhibitor which completely eliminated internalisation: it is likely that internalisation occurs through more than one single mechanism. It is also worth noting that standard deviations among the 4 experiments were more important in the case of liposomes: surprisingly, it seems that EVs have a more stable, predicable behaviour than their synthetic liposomal counterparts. This may seem counterintuitive as one might expect synthetic nanoparticles to behave more consistently than biological vesicles; it is nevertheless one more advantage EVs may present.

With the objective of fine-tuning EVs as synthetic vectors, and of switching the biological point of view on EVs to a more physico-chemical one, we chose to consider several physical processes to load EVs. We aimed at characterising the effect of these methods (sonication, extrusion, freeze drying) and determining their impact on EV size, concentration and structure (Figure 6) as well as internalisation *in vitro* (Figure 8). We performed extrusion on 50 nm membranes with the goal of inducing membrane reshaping, considering the initial size of EVs (slightly inferior to 100 nm). Surprisingly, whereas EV membrane was previously reported to be rigid and our own lipidomics results evidenced a high amount of PC, a lipid known to induce membrane rigidity, we managed to extrude EVs at room temperature through 50 nm membranes. To our knowledge, this had never been described before. Extrusion reduced EV size and narrowed size distribution as visible in the decrease of SD (Figure 6A) and the changes to the distribution profile (Figure 6B): this conflicts with the findings of Fuhrmann *et al.* [2] who observed a widening of peak distribution when using this method to load porphyrins. CryoTEM imaging showed EVs retained their spherical structure after extrusion, although vesicles were smaller (Figure 6C). Haney *et al.* on the other hand observed round EVs, but saw an increase in size. These differences could be explained by the difference in pore size used*:* 400 nm [2] and 200 nm [11] vs. 50 nm in this study. Importantly, we observed that extrusion did not affect EV internalisation properties (Figure 8). Sonication probe on the other hand lowered

EV concentration (Figure 6A). It increased EV internalisation (Figure 8), which is consistent with the results obtained by Haney *et al.* [11]. Sonication seemed nevertheless detrimental to EV structure integrity, as cryoTEM images revealed multiple EVs to have lost their spherical shape (Figure 6C). With the goal of creating a dried EV film which can be rehydrated with a solution of drugs, we also investigate effect of freeze drying on cell internalisation. Interestingly, freeze-drying had no significant impact on internalisation (Figure 8). Additionally, these three physical modifications did not impact the endocytic pathway EVs follow during cell internalisation (Figure S11). Considering these results, we deemed extrusion, associated or not with freeze drying, more promising than sonication as a future method to allow the loading of chemicals or even biomolecules. Nevertheless, it is important to note that despite potential expectations concerning their *in vivo* stability, when administered in a non autologous host, EVs are quickly eliminated ($t_{1/2}$ = 2 min [85, 86]) and found in elimination organs, following classic behaviour of synthetic vectors [87, 88]. In this context, still focusing on EVs as synthetic systems, surface modifications (polymer stabilisation or targeting), as described by Schiffelers's group [89, 90] and others [91], also represent a challenging broad research axis.

## Conclusion

EVs hold great promise as a drug delivery platform, given their convincing *in vivo* results [6-8]. Nevertheless, a broad use of such vesicles is not yet an option, especially in regards to feasibility issues. Here, we isolated and thoroughly characterised mMSC-derived EVs in terms of size, concentration (in particles per mL and protein concentration), structure, protein, lipid and miRNA content. Importantly, we first focused on the comprehension of EV colloidal behaviour to establish handling protocols, and allow a convenient use of such vesicles, almost as easily as with synthetic vesicles such as liposomes. We determined freezing at -80°C in trehalose with or without protease inhibitors allowed satisfactory EV storage. We explored freeze-drying as a storage solution and found optimal conditions in terms of freezing volume, concentration and buffer. We identified extrusion and freeze-drying as interesting and promising processes which could be basic steps for future cargo loading into EVs, while not compromising EV structure, protein content or size, nor impacting their internalisation abilities. More importantly, EVs proved to have greater internalisation capabilities *in vitro* compared to commercial standard liposomes, establishing their interest in comparison to such synthetic vesicles, probably explained by the observed difference in endocytic pathway. This is a clear advantage of such natural vesicles compared to their synthetic counterparts, and the careful

identification of crucial handling protocols could help imagine them as a basis for future drug delivery platforms.

**Acknowledgements**

The authors would like to thank Danièle Noël and her team (IRMB, INSERM U1183, Montpellier) for kindly providing us with mesenchymal stem cells, as well as Nicolas Donzel (AIME, ICGM, CNRS, Montpellier) for access to the Optima XPN-80 Ultracentrifuge (Beckman Coulter), and Céline Salsac and Cédric Raoul (INM, INSERM UMR1051, Montpellier) for access to the BD Accuri C6 flow cytometer. This work was supported by Centre national de la recherche scientifique (CNRS) and Université de Montpellier, as well as INCa-Cancéropôle GSO. The cryoTEM platform is supported by the French Infrastructure for Integrated Structural Biology, a national infrastructure supported by the French National Research Agency (ANR-10-INBS-05). The MRI facility is supported by ANR grant (ANR-10-INBS-04).

**Competing interests statement**

The authors have no competing interests to declare.

**Data availability statement**

All the data used to draw the conclusions of this paper are present in the data presented in the figures and/or supplementary figures; raw transcriptomics data are available in the NCBI data base under GEO number ####. The raw/processed data required to reproduce these findings are available from the corresponding author upon request.

**Bibliography**


1. Johnsen, K.B., et al., *A comprehensive overview of exosomes as drug delivery vehicles - endogenous nanocarriers for targeted cancer therapy.* Biochimica et Biophysica Acta, 2014. **1846**(1): p. 75-87.
2. Fuhrmann, G., et al., *Active loading into extracellular vesicles significantly improves the cellular uptake and photodynamic effect of porphyrins.* Journal of Controlled Release, 2015. **205**: p. 35-44.
3. Gomari, H., M. Forouzandeh Moghadam, and M. Soleimani, *Targeted cancer therapy using engineered exosome as a natural drug delivery vehicle.* OncoTargets and Therapy, 2018. **11**: p. 5753-5762.
4. van Niel, G., G. D'Angelo, and G. Raposo, *Shedding light on the cell biology of extracellular vesicles.* Nature Reviews Molecular Cell Biology, 2018. **19**(4): p. 213-228.
5. French, K.C., M.A. Antonyak, and R.A. Cerione, *Extracellular vesicle docking at the cellular port: Extracellular vesicle binding and uptake.* Seminars in Cell & Developmental Biology, 2017. **67**: p. 48-55.
6. Kamerkar, S., et al., *Exosomes facilitate therapeutic targeting of oncogenic KRAS in pancreatic cancer.* Nature, 2017. **546**(7659): p. 498-503.
7. Alvarez-Erviti, L., et al., *Delivery of siRNA to the mouse brain by systemic injection of targeted exosomes.* Nature Biotechnology, 2011. **29**(4): p. 341-5.
8. Armstrong, J.P.K. and M.M. Stevens, *Strategic design of extracellular vesicle drug delivery systems.* Advanced Drug Delivery Reviews, 2018. **130**: p. 12-16.
9. Zhuang, X., et al., *Treatment of brain inflammatory diseases by delivering exosome encapsulated anti-inflammatory drugs from the nasal region to the brain.* Molecular Therapy : the Journal of the American Society of Gene Therapy, 2011. **19**(10): p. 1769-79.
10. Kooijmans, S.A.A., et al., *Electroporation-induced siRNA precipitation obscures the efficiency of siRNA loading into extracellular vesicles.* Journal of Controlled Release, 2013. **172**(1): p. 229-238.
11. Haney, M.J., et al., *Exosomes as drug delivery vehicles for Parkinson's disease therapy.* Journal of Controlled Release, 2015. **207**: p. 18-30.
12. Kim, M.S., et al., *Development of exosome-encapsulated paclitaxel to overcome MDR in cancer cells.* Nanomedicine : Nanotechnology, Biology, and Medicine, 2016. **12**(3): p. 655-664.
13. Thery, C., et al., *Minimal information for studies of extracellular vesicles 2018 (MISEV2018): a position statement of the International Society for Extracellular Vesicles and update of the MISEV2014 guidelines.* Journal of Extracellular Vesicles, 2018. **7**(1): p. 1535750.
14. Ingato, D., et al., *Good things come in small packages: Overcoming challenges to harness extracellular vesicles for therapeutic delivery.* Journal of Controlled Release, 2016. **241**: p. 174-185.
15. de Jong, O.G., et al., *Cellular stress conditions are reflected in the protein and RNA content of endothelial cell-derived exosomes.* Journal of Extracellular Vesicles, 2012. **1**.
16. Zhou, J., et al., *Mesenchymal Stem Cell Derived Exosomes in Cancer Progression, Metastasis and Drug Delivery: A Comprehensive Review.* Journal of Cancer, 2018. **9**(17): p. 3129-3137.
17. Kalimuthu, S., et al., *A New Approach for Loading Anticancer Drugs Into Mesenchymal Stem Cell-Derived Exosome Mimetics for Cancer Therapy.* Frontiers in Pharmacology, 2018. **9**: p. 1116.
18. Kordelas, L., et al., *MSC-derived exosomes: a novel tool to treat therapy-refractory graft-versus-host disease.* Leukemia, 2014. **28**(4): p. 970-3.
19. Frank, J., et al., *Extracellular vesicles protect glucuronidase model enzymes during freeze-drying.* Scientific Reports, 2018. **8**(1): p. 12377.

20. Raisin, S., et al., *Tripartite polyionic complex (PIC) micelles as non-viral vectors for mesenchymal stem cell siRNA transfection.* Biomaterials Science, 2017. **5**(9): p. 1910-1921.
21. Chang, H.-I. and M.-K. Yeh, *Clinical development of liposome-based drugs: formulation, characterization, and therapeutic efficacy.* International Journal of Nanomedicine, 2012. **7**: p. 49-60.
22. Bulbake, U., et al., *Liposomal Formulations in Clinical Use: An Updated Review.* Pharmaceutics, 2017. **9**(2).
23. Hartmann, E.M., et al., *Taking the shortcut for high-throughput shotgun proteomic analysis of bacteria.* Methods in Molecular Biology, 2014. **1197**: p. 275-85.
24. Klein, G., et al., *RNA-binding proteins are a major target of silica nanoparticles in cell extracts.* Nanotoxicology, 2016. **10**(10): p. 1555-1564.
25. Bligh, E.G. and W.J. Dyer, *A rapid method of total lipid extraction and purification.* Canadian Journal of Biochemistry and Physiology, 1959. **37**(8): p. 911-7.
26. Barrans, A., et al., *Hepatic lipase induces the formation of pre-beta 1 high density lipoprotein (HDL) from triacylglycerol-rich HDL2. A study comparing liver perfusion to in vitro incubation with lipases.* The Journal of Biological Chemistry, 1994. **269**(15): p. 11572-7.
27. Le Faouder, P., et al., *LC-MS/MS method for rapid and concomitant quantification of pro-inflammatory and pro-resolving polyunsaturated fatty acid metabolites.* Journal of Chromatography B, Analytical Technologies in the Biomedical and Life Sciences, 2013. **932**: p. 123-33.
28. Martin, M., *Cutadapt removes adapter sequences from high-throughput sequencing reads.* 2011, 2011. **17**(1): p. 3.
29. Andres-Leon, E., R. Nunez-Torres, and A.M. Rojas, *miARma-Seq: a comprehensive tool for miRNA, mRNA and circRNA analysis.* Sci Rep, 2016. **6**: p. 25749.
30. Gentleman, R.C., et al., *Bioconductor: open software development for computational biology and bioinformatics.* Genome Biol, 2004. **5**(10): p. R80.
31. Robinson, M.D., D.J. McCarthy, and G.K. Smyth, *edgeR: a Bioconductor package for differential expression analysis of digital gene expression data.* Bioinformatics, 2010. **26**(1): p. 139-40.
32. Anders, S. and W. Huber, *Differential expression analysis for sequence count data.* Genome Biol, 2010. **11**(10): p. R106.
33. Love, M.I., W. Huber, and S. Anders, *Moderated estimation of fold change and dispersion for RNA-seq data with DESeq2.* Genome Biol, 2014. **15**(12): p. 550.
34. Kowal, J., et al., *Proteomic comparison defines novel markers to characterize heterogeneous populations of extracellular vesicle subtypes.* Proceedings of the National Academy of Sciences of the United States of America, 2016. **113**(8): p. E968-77.
35. Meehan, B., J. Rak, and D. Di Vizio, *Oncosomes - large and small: what are they, where they came from?* Journal of Extracellular Vesicles, 2016. **5**.
36. Rana, S., et al., *Toward tailored exosomes: the exosomal tetraspanin web contributes to target cell selection.* The International Journal of Biochemistry & Cell Biology, 2012. **44**(9): p. 1574-84.
37. Hemler, M.E., *Tetraspanin functions and associated microdomains.* Nature Reviews Molecular Cell Biology, 2005. **6**(10): p. 801-11.
38. Hemler, M.E., *Tetraspanin proteins mediate cellular penetration, invasion, and fusion events and define a novel type of membrane microdomain.* Annu Rev Cell Dev Biol, 2003. **19**: p. 397-422.
39. Carvalho, P.C., et al., *PatternLab for proteomics: a tool for differential shotgun proteomics.* BMC Bioinformatics, 2008. **9**: p. 316.
40. Tzeng, S.Y., et al., *Cystamine-terminated poly(beta-amino ester)s for siRNA delivery to human mesenchymal stem cells and enhancement of osteogenic differentiation.* Biomaterials, 2012. **33**(32): p. 8142-51.

41. Morigele, M., et al., *TGF-beta1 induces a nucleus pulposus-like phenotype in Notch 1 knockdown rabbit bone marrow mesenchymal stem cells.* Cell Biology International, 2013. **37**(8): p. 820-5.
42. Zhang, J.-f., et al., *MiRNA-20a promotes osteogenic differentiation of human mesenchymal stem cells by co-regulating BMP signaling.* RNA Biology, 2011. **8**(5): p. 829-38.
43. Maas, S.L.N., X.O. Breakefield, and A.M. Weaver, *Extracellular Vesicles: Unique Intercellular Delivery Vehicles.* Trends in Cell Biology, 2017. **27**(3): p. 172-188.
44. Cheng, L., et al., *Focus on Mesenchymal Stem Cell-Derived Exosomes: Opportunities and Challenges in Cell-Free Therapy.* Stem Cells International, 2017. **2017**: p. 6305295.
45. Escrevente, C., et al., *Interaction and uptake of exosomes by ovarian cancer cells.* BMC Cancer, 2011. **11**: p. 108.
46. Haraszti, R.A., et al., *High-resolution proteomic and lipidomic analysis of exosomes and microvesicles from different cell sources.* Journal of Extracellular Vesicles, 2016. **5**: p. 32570.
47. *Vesiclepedia, http://www.microvesicles.org/, accessed March 2017*.
48. Skotland, T., K. Sandvig, and A. Llorente, *Lipids in exosomes: Current knowledge and the way forward.* Progress in Lipid Research, 2017. **66**: p. 30-41.
49. Llorente, A., et al., *Molecular lipidomics of exosomes released by PC-3 prostate cancer cells.* Biochimica et Biophysica Acta, 2013. **1831**(7): p. 1302-9.
50. Trajkovic, K., et al., *Ceramide triggers budding of exosome vesicles into multivesicular endosomes.* Science (New York, N Y ), 2008. **319**(5867): p. 1244-7.
51. Wubbolts, R., et al., *Proteomic and biochemical analyses of human B cell-derived exosomes - Potential implications for their function and multivesicular body formation.* Journal of Biological Chemistry, 2003. **278**(13): p. 10963-10972.
52. Laulagnier, K., et al., *Mast cell- and dendritic cell-derived exosomes display a specific lipid composition and an unusual membrane organization.* The Biochemical Journal, 2004. **380**(Pt 1): p. 161-71.
53. Vidal, M., et al., *Asymmetric distribution of phospholipids in the membrane of vesicles released during in vitro maturation of guinea pig reticulocytes: evidence precluding a role for "aminophospholipid translocase".* Journal of Cellular Physiology, 1989. **140**(3): p. 455-62.
54. Phuyal, S., et al., *The ether lipid precursor hexadecylglycerol stimulates the release and changes the composition of exosomes derived from PC-3 cells.* The Journal of Biological Chemistry, 2015. **290**(7): p. 4225-37.
55. Brouwers, J.F., et al., *Distinct lipid compositions of two types of human prostasomes.* Proteomics, 2013. **13**(10-11): p. 1660-6.
56. Record, M., et al., *Extracellular vesicles: lipids as key components of their biogenesis and functions.* Journal of Lipid Research, 2018. **59**(8): p. 1316-1324.
57. Li, J., et al., *miR-10a restores human mesenchymal stem cell differentiation by repressing KLF4.* J Cell Physiol, 2013. **228**(12): p. 2324-36.
58. Huang, S., et al., *Upregulation of miR-22 promotes osteogenic differentiation and inhibits adipogenic differentiation of human adipose tissue-derived mesenchymal stem cells by repressing HDAC6 protein expression.* Stem Cells Dev, 2012. **21**(13): p. 2531-40.
59. Zhang, F.X., et al., *microRNA-10b promotes the migration of mouse bone marrow-derived mesenchymal stem cells and downregulates the expression of E-cadherin.* Molecular Medicine Reports, 2013. **8**(4): p. 1084-1088.
60. Zhao, X., et al., *The toll-like receptor 3 ligand, poly(I:C), improves immunosuppressive function and therapeutic effect of mesenchymal stem cells on sepsis via inhibiting MiR-143.* Stem Cells, 2014. **32**(2): p. 521-33.
61. Baglio, S.R., et al., *Human bone marrow- and adipose-mesenchymal stem cells secrete exosomes enriched in distinctive miRNA and tRNA species.* Stem Cell Res Ther, 2015. **6**: p. 127.
62. Katakowski, M., et al., *Exosomes from marrow stromal cells expressing miR-146b inhibit glioma growth.* Cancer Lett, 2013. **335**(1): p. 201-4.

63. Katakowski, M., et al., *MiR-146b-5p suppresses EGFR expression and reduces in vitro migration and invasion of glioma.* Cancer Invest, 2010. **28**(10): p. 1024-30.
64. Xu, Y., et al., *microRNA-16-5p-containing exosomes derived from bone marrow-derived mesenchymal stem cells inhibit proliferation, migration, and invasion, while promoting apoptosis of colorectal cancer cells by downregulating ITGA2.* Journal of Cellular Physiology, 2019. **234**(11): p. 21380-21394.
65. Lee, J.K., et al., *Exosomes Derived from Mesenchymal Stem Cells Suppress Angiogenesis by Down-Regulating VEGF Expression in Breast Cancer Cells.* Plos One, 2013. **8**(12).
66. Wang, X., et al., *Exosomal miR-223 Contributes to Mesenchymal Stem Cell-Elicited Cardioprotection in Polymicrobial Sepsis.* Sci Rep, 2015. **5**: p. 13721.
67. Shao, L.B., et al., *MiRNA-Sequence Indicates That Mesenchymal Stem Cells and Exosomes Have Similar Mechanism to Enhance Cardiac Repair.* Biomed Research International, 2017.
68. Feng, Y.L., et al., *Ischemic Preconditioning Potentiates the Protective Effect of Stem Cells through Secretion of Exosomes by Targeting Mecp2 via miR-22.* Plos One, 2014. **9**(2).
69. Yu, B., et al., *Cardiomyocyte Protection by GATA-4 Gene Engineered Mesenchymal Stem Cells Is Partially Mediated by Translocation of miR-221 in Microvesicles.* Plos One, 2013. **8**(8).
70. Ma, T., et al., *MicroRNA-132, Delivered by Mesenchymal Stem Cell-Derived Exosomes, Promote Angiogenesis in Myocardial Infarction.* Stem Cells International, 2018. **2018**: p. 11.
71. Thery, C., et al., *Minimal information for studies of extracellular vesicles 2018 (MISEV2018): a position statement of the International Society for Extracellular Vesicles and update of the MISEV2014 guidelines.* Journal of Extracellular Vesicles, 2019. **8**(1): p. 43.
72. Tang, K., et al., *Delivery of chemotherapeutic drugs in tumour cell-derived microparticles.* Nature Communications, 2012. **3**: p. 1282.
73. Lee M., B.J.-J., Im W., Kim M., *Influence of storage condition on exosome recovery.* Biotechnology and Bioprocess Engineering, 2016. **21**(2): p. 299-304.
74. Kalra, H., et al., *Comparative proteomics evaluation of plasma exosome isolation techniques and assessment of the stability of exosomes in normal human blood plasma.* Proteomics, 2013. **13**(22): p. 3354-64.
75. Bosch, S., et al., *Trehalose prevents aggregation of exosomes and cryodamage.* Scientific Reports, 2016. **6**: p. 36162.
76. Charoenviriyakul, C., et al., *Preservation of exosomes at room temperature using lyophilization.* International Journal of Pharmaceutics, 2018. **553**(1-2): p. 1-7.
77. Akers, J.C., et al., *Optimizing preservation of extracellular vesicular miRNAs derived from clinical cerebrospinal fluid.* Cancer Biomarkers : Section A of Disease Markers, 2016. **17**(2): p. 125-32.
78. Cheng, X.W. and R.J. Lee, *The role of helper lipids in lipid nanoparticles (LNPs) designed for oligonucleotide delivery.* Advanced Drug Delivery Reviews, 2016. **99**: p. 129-137.
79. Wan, C., T.M. Allen, and P.R. Cullis, *Lipid nanoparticle delivery systems for siRNA-based therapeutics.* Drug Delivery and Translational Research, 2014. **4**(1): p. 74-83.
80. Mulcahy, L.A., R.C. Pink, and D.R. Carter, *Routes and mechanisms of extracellular vesicle uptake.* Journal of Extracellular Vesicles, 2014. **3**.
81. Morelli, A.E., et al., *Endocytosis, intracellular sorting, and processing of exosomes by dendritic cells.* Blood, 2004. **104**(10): p. 3257-66.
82. Montecalvo, A., et al., *Mechanism of transfer of functional microRNAs between mouse dendritic cells via exosomes.* Blood, 2012. **119**(3): p. 756-66.
83. Svensson, K.J., et al., *Exosome uptake depends on ERK1/2-heat shock protein 27 signaling and lipid Raft-mediated endocytosis negatively regulated by caveolin-1.* The Journal of Biological Chemistry, 2013. **288**(24): p. 17713-24.
84. Izquierdo-Useros, N., et al., *Capture and transfer of HIV-1 particles by mature dendritic cells converges with the exosome-dissemination pathway.* Blood, 2009. **113**(12): p. 2732-41.

85. Takahashi, Y., et al., *Visualization and in vivo tracking of the exosomes of murine melanoma B16-BL6 cells in mice after intravenous injection.* Journal of Biotechnology, 2013. **165**(2): p. 77-84.
86. Smyth, T., et al., *Biodistribution and delivery efficiency of unmodified tumor-derived exosomes.* Journal of Controlled Release, 2015. **199**: p. 145-155.
87. Wiklander, O.P.B., et al., *Extracellular vesicle in vivo biodistribution is determined by cell source, route of administration and targeting.* Journal of extracellular vesicles, 2015. **4**: p. 26316-26316.
88. Morishita, M., et al., *Quantitative Analysis of Tissue Distribution of the B16BL6-Derived Exosomes Using a Streptavidin-Lactadherin Fusion Protein and Iodine-125-Labeled Biotin Derivative After Intravenous Injection in Mice.* Journal of Pharmaceutical Sciences, 2015. **104**(2): p. 705-713.
89. Kooijmans, S.A.A., et al., *Display of GPI-anchored anti-EGFR nanobodies on extracellular vesicles promotes tumour cell targeting.* Journal of Extracellular Vesicles, 2016. **5**.
90. Kooijmans, S.A.A., et al., *PEGylated and targeted extracellular vesicles display enhanced cell specificity and circulation time.* Journal of Controlled Release, 2016. **224**: p. 77-85.
91. Smyth, T., et al., *Surface Functionalization of Exosomes Using Click Chemistry.* Bioconjugate Chemistry, 2014. **25**(10): p. 1777-1784.

**List of figures**

**A.**

| | Mean ± SD |
|---|---|
| Hydrodynamic diameter (NTA mode, nm) | 94.4 ± 10.3 |
| Surface charge (zeta potential, mV) | -15 ± 2 |
| Number of EVs / $10^6$ cells (NTA) | 9.7 ± 3.5 x $10^8$ |
| Protein quantity / $10^6$ cells (BCA, µg) | 2.2 ± 1.0 |
| Protein quantity / $10^{10}$ EVs (BCA / NTA, µg) | 22.7 ± 5.7 |

**B.**

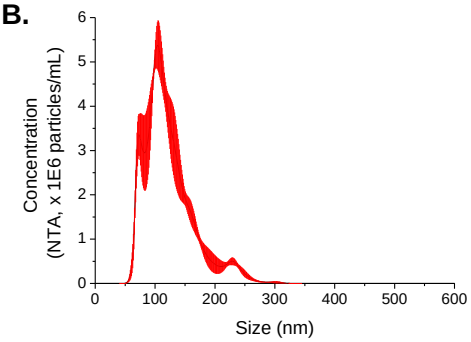


**C.**

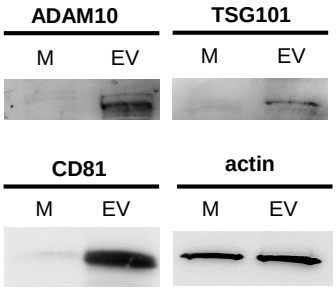


**D.**

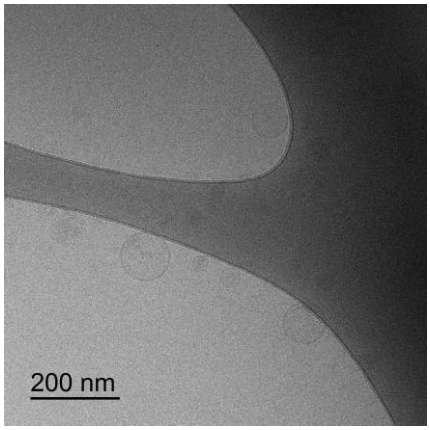


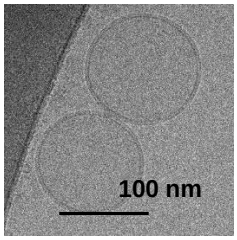


**Figure 1 – Characterisation of mMSC-derived EVs. A. Quantification (NTA, microBCA analysis)**. The number of producing mMSC was assessed during EV isolation. Measurements were performed on 20 independent EV batches, except the surface charge which was measured for 4 independent EV batches. Results are expressed as the mean ± SD of the batches. **B. NTA analysis.** Size distribution and concentration of a representative EV batch. **C. Western blotting**. M: mMSC cell lysate. 2.5 µg total protein loaded. Chemiluminescence exposure time: 30 seconds - 1 min. Protein expression of small EV associated-markers ADAM10, TSG101 and CD81 was assessed on 4 independent EV batches. **D. CryoTEM**. EV structure was observed. Representative images, from an EV batch kept at 4°C for 5 days in PBS, are shown. CryoTEM analysis was performed on 5 independent EV batches.

**A.**

| Protein categories (from Théry *et al.*, 2018) | | Proteins identified in mMSC derived-EV samples |
|---|---|---|
| 1. Transmembrane or GPI-anchored proteins associated to plasma membrane and/or endosomes | 1a. Non-tissue specific | Tetraspanins CD81, CD82, CD63; integrins; ADAM10; CD47; galectins; phospholipid scramblases |
| | 1b. Cell/tissue specific | CD9 |
| 2. Cytosolic proteins | 2a. With lipid or membrane protein-binding ability | ESCRT associated proteins TSG101, Alix, Vps4; syntenin-1; EHD4; annexins; flotillin-2; clathrin; Rab proteins |
| | 2b. Promiscuous incorporation in EVs | Heat shock proteins HSP70, HSP90; cytoskeletal proteins actin, tubulin; peroxidorexins; glutathione S-transferases |
| 3. Major components of non-EV co-isolated structure | 3a. Lipoproteins | *Not detected: apolipoproteins A1/2 and B; albumin* |
| | 3b. Proteins | Ribosomal proteins (52)<br>*Not detected: ribosomal proteins; complement proteins* |
| 4. Transmembrane, lipid-bound and soluble proteins associated to other intracellular compartments than PM/endosomes | 4a. Nucleus | Histones, histone-associated proteins<br>*Not detected: lamin A/C, eEF2, MVP* |
| | 4b. Mitochondria | Mitochondria-associated precursor proteins (11); mitochondrial histones (histone 4)<br>*Not detected: cytochrome c, IMMT, TOMM20, mitofilin* |
| | 4c. Secretory pathway | Golgi apparatus protein 1 precursor<br>*Not detected: endoplasmic reticulum markers calnexin, calreticulin, GP96, HSPA5; Golgi protein GOLGA2* |
| | 4d. Others (autophagosomes, cytoskeleton…) | Actinin1/4 (ACTN1/4)<br>*Not detected: autophagy-related ATG9A; cytokeratin 18 (KRT18)* |
| 5. Secreted proteins recovered with EVs | 5a. Cytokines and growth factors | Osteoclast-stimulating factor 1<br>*Not detected: stress-related protein MIF Macrophage migration inhibitory factor; VEGF, TGF, IFN, FGF, PEDGF, EGF, HGF, MMP1, TIMP2; interleukins (IL6)* |
| | 5b. Adhesion and extracellular matrix proteins | Collagen-related precursors and pre-preproteins; PEDF precursor |

**B.**

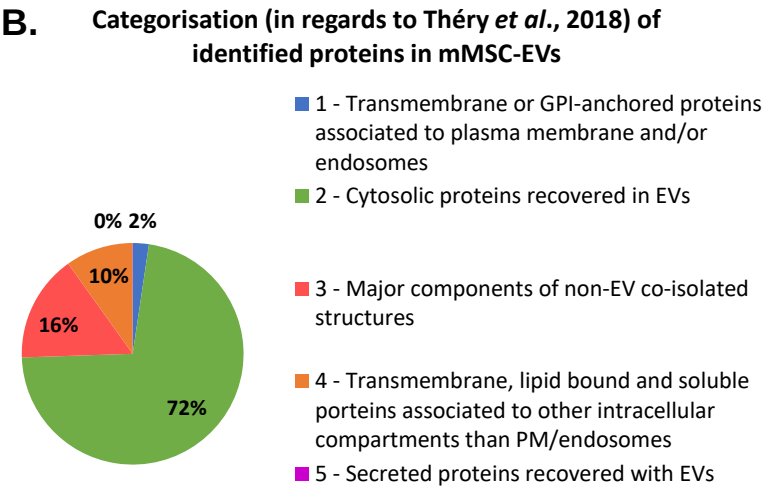


**C.**

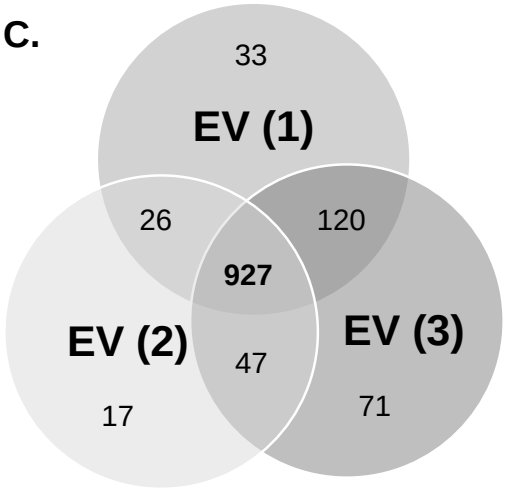


**Figure 2 – Proteomics analysis of mMSC-derived EVs.** Protein content was assessed for EVs of 3 independent batches (20 µg protein/analysis). Proteins considered are the ones validated with at least 2 different peptides (1,241 proteins). **A. Proteomics analysis summary**. Proteins categories are the ones described in Théry *et al.*, 2018. **B. Proportions represented by each protein category.** Percentages were calculated from %NSAF (normalised spectral abundance factor) of proteins and precursors. **C. Venn diagramme comparing the 3 EV batches**. EV(X): EV batch number X. The numbers indicated are the number of proteins comprised in each section. For instance, 927 proteins are common to all three EV batches.

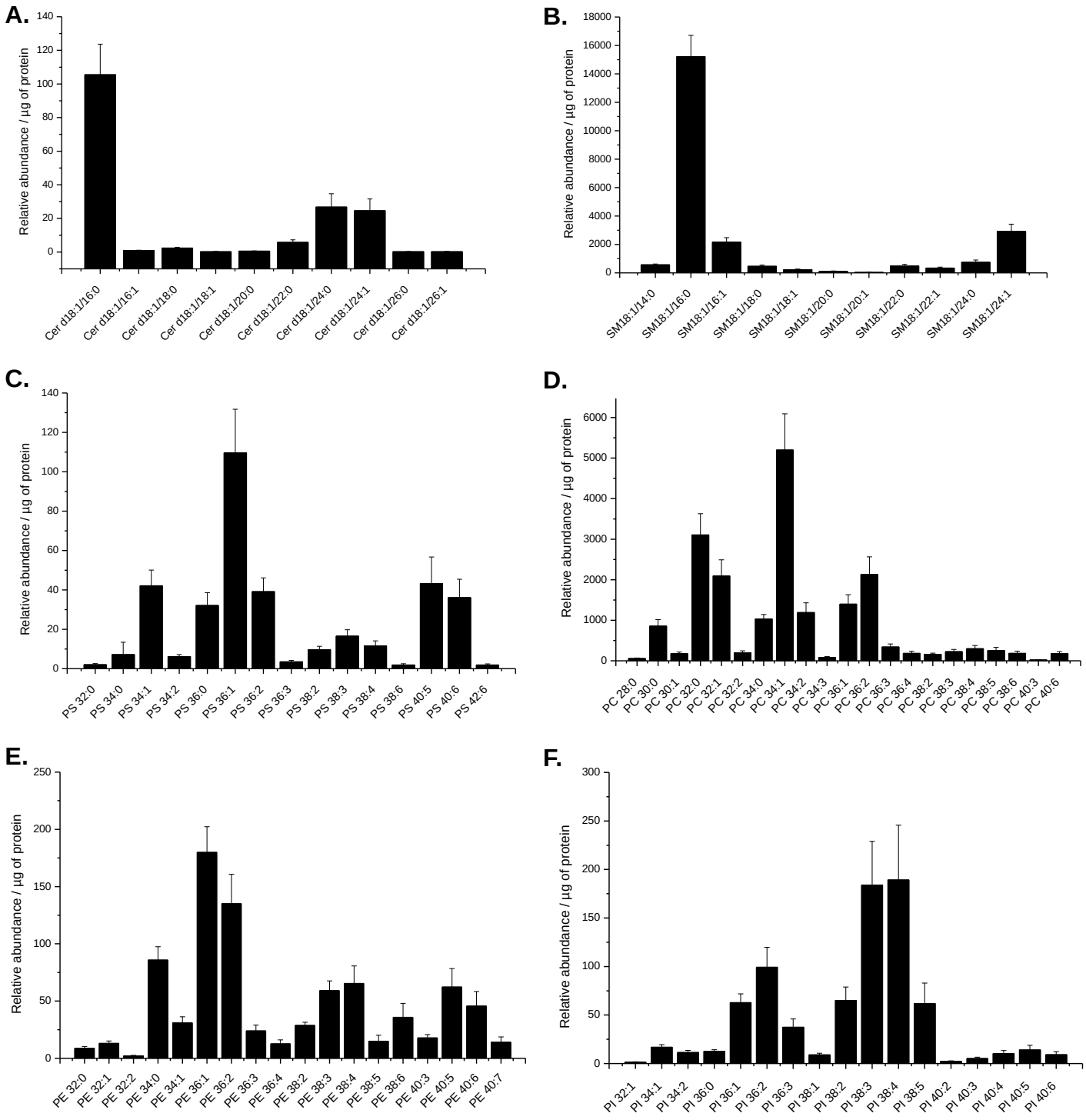


**Figure 3 – Lipidomics analysis of mMSC-derived EVs.** Lipid content was assessed for EVs of 3 different batches. Results are expressed as the mean ± SD of the batches. Results are presented by lipid classes, and expressed as relative abundance (ratio area of detected species/area of the internal standard) normalised by µg of protein. X:Y expresses the number X of carbons in the fatty acid chains and the number Y of unsaturations. **A. Ceramides** (Cer); **B. Sphingomyelins** (SM); **C. Phosphatidylserines** (PS); **D. Phosphatidylcholines** (PC); **E. Phosphatidylethanolamines** (PE); **F. Phosphatidylinositols** (PI).

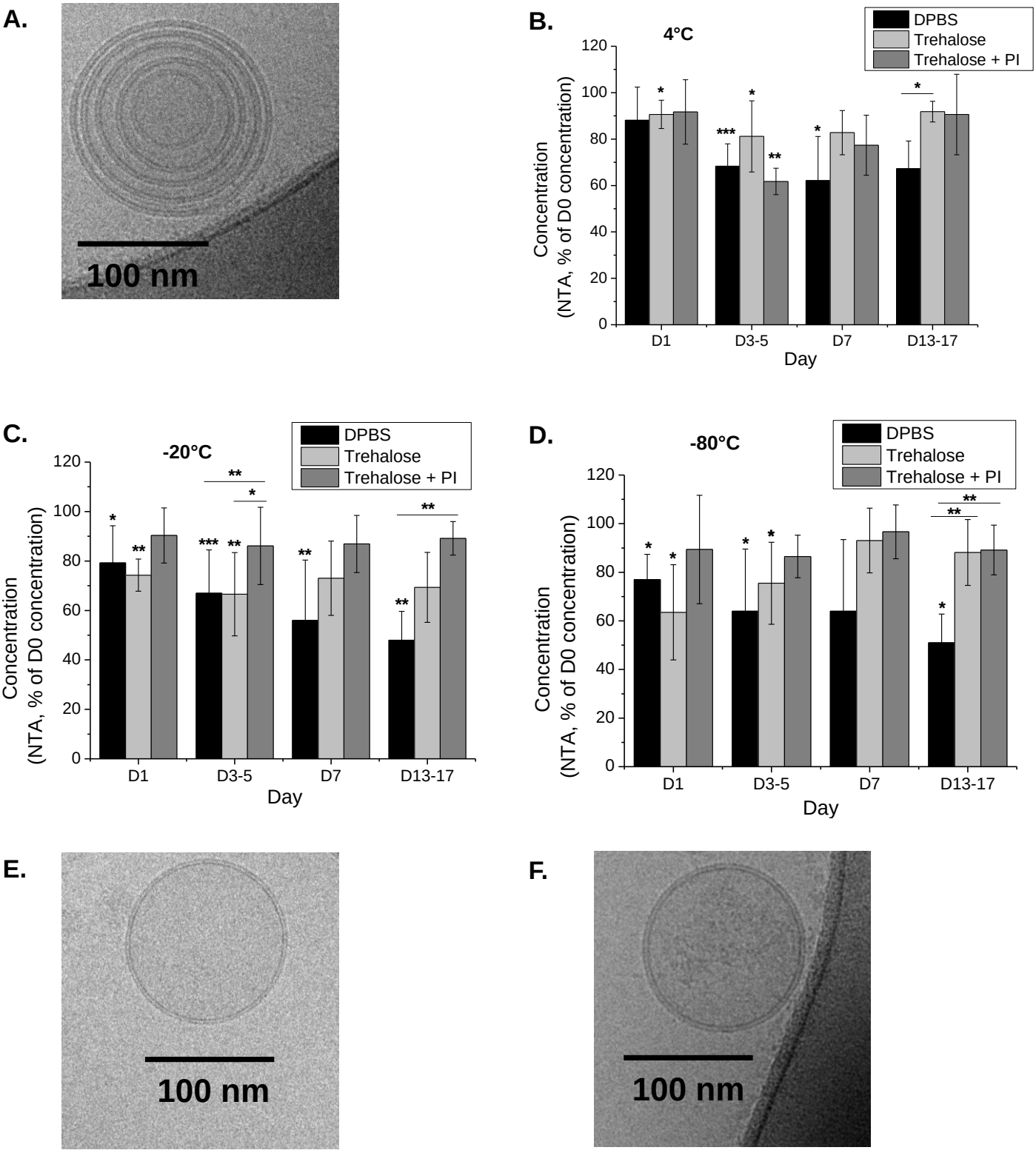


**Figure 4 – Conservation of EVs. A. CryoTEM image of freeze-thawed EVs.** EVs were frozen at -20°C in DPBS and went through at least 2 freeze-thaw cycles before analysis. **B-D.** EVs were resuspended in the chosen buffer (DPBS, trehalose 25 mM, trehalose 25 mM + protease inhibitors (PI)) on the final day of EV isolation, after NTA analysis. On day X (DX), the EV aliquot was thawed, diluted appropriately and analysed by NTA. EV concentration (measured in particles/mL) on DX is expressed as a percentage of EV concentration after isolation, on day 0 (D0). All conditions (temperature, day) and measurements were performed on at least 3 independent EV batches. Results are expressed as the mean ± SD of the batches. One-sample t-tests were performed to compare each percentage to the theoretical value of 100%, which corresponds to perfect storage conditions with no EV concentration loss; two-sample t-tests were performed to compare percentages two by two (* : $p<0.05$, ** : $p<0.01$, *** : $p<0.001$). **Freezing at A. 4°C**. **B. -20°C**. **C. -80°C. E&F. CryoTEM images of EVs frozen at -80°C in E. trehalose 25 mM** (thawed on D60)**. F. trehalose 25 mM + PI** (thawed on D60)**.**

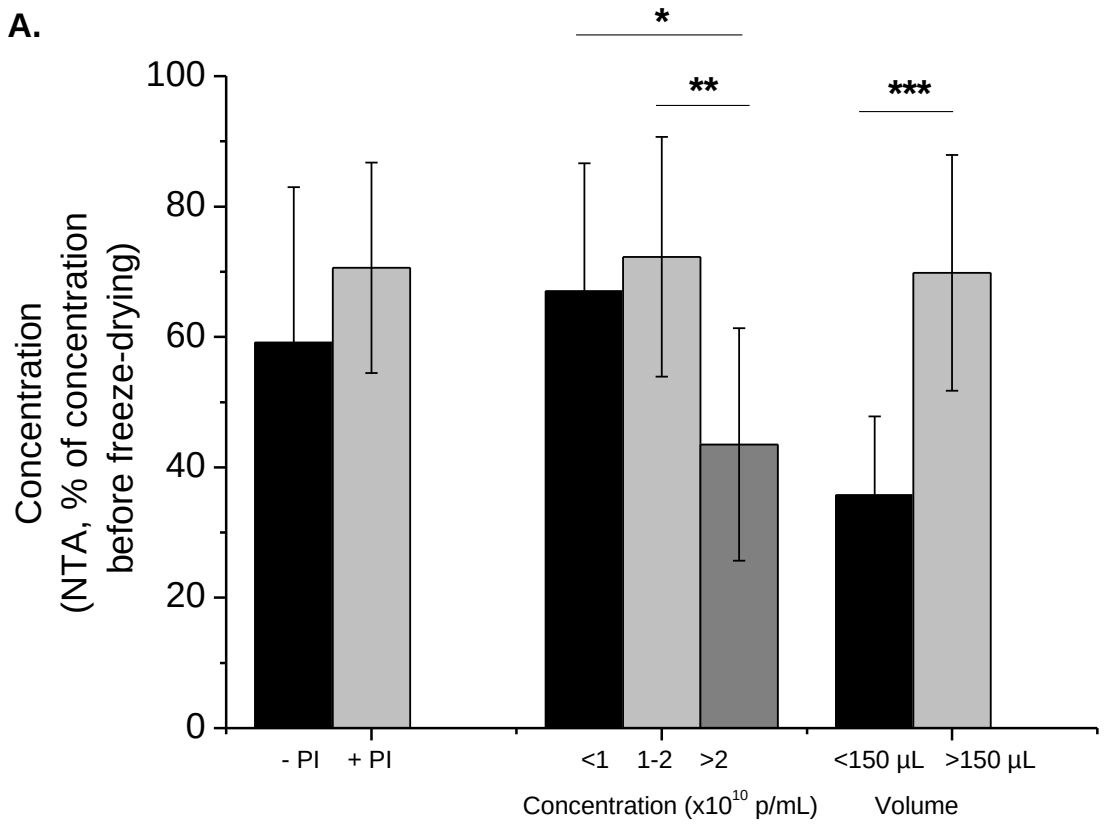


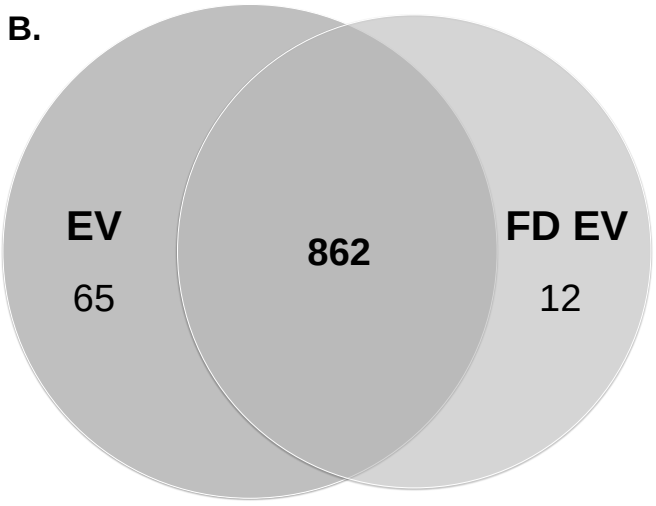


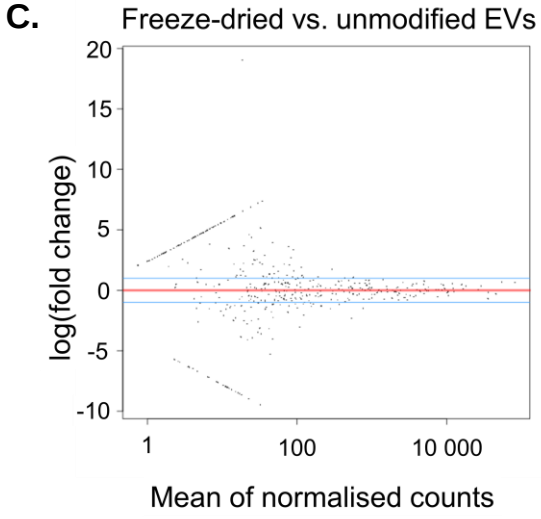


**Figure 5 – Conservation of EVs by freeze-drying. A. Concentration conservation measured by NTA.** EVs were frozen at -80°C in trehalose ± PI, at a concentration <1, 1-2 or >2 x $10^{10}$ particles /mL and in a volume <150 µL or >150 µL, and dried overnight. EV concentration (measured in particles/mL) is expressed as a percentage of EV concentration before freeze-drying. Results are expressed as the mean ± SD of at least 6 independent experiments. Two-sample t-tests were performed to compare percentages two by two (* : $p<0.05$, ** : $p<0.01$, *** : $p<0.001$). **B. Venn diagramme of proteomics analysis of freeze-dried EVs vs. unmodified EVs.** EV: proteins common to all three unmodified EV batches; FD EV: proteins present in freeze-dried EVs (one batch). The numbers indicated are the number of proteins comprised in each section. For instance, 862 proteins are common to all three EV batches and freeze-dried EVs. **C. Statistical analysis of transcriptomics data of freeze-dried EVs vs. unmodified EVs.** MiRNAs were considered for this analysis when the sum of raw counts associated with the miRNA across the 5 samples (2 unmodified EV batches, 3 freeze-dried EV batches) was above an arbitrary threshold of 15. The fold change of the mean of normalised counts for freeze-dried EVs against the mean of normalised counts for unmodified EVs was calculated. The log of the fold change was plotted against the mean of normalised counts. No differentially expressed miRNA were detected.

**A.**

| | Extrusion (n=4) | | Sonication (n=3) | | Freeze-drying (n=4) | |
|---|---|---|---|---|---|---|
| | **Before** | **After** | **Before** | **After** | **Before** | **After** |
| Mode (nm) | 100 ± 9 | 79 ± 7 ** | 94 ± 1 | 80 ± 3 * | 99 ± 13 | 101 ± 11 |
| Mean (nm) | 123 ± 4 | 96 ± 19 * | 121 ± 5 | 102 ± 1 * | 120 ± 3 | 134 ± 4 * |
| SD (nm) | 41 ± 3 | 34 ± 19 | 43 ± 2 | 32 ± 1 ** | 38 ± 1 | 51 ± 1 *** |
| Concentration (% before) | 100 | 116 ± 40 | 100 | 66 ± 13 * | 100 | 77 ± 12 * |

**B.**

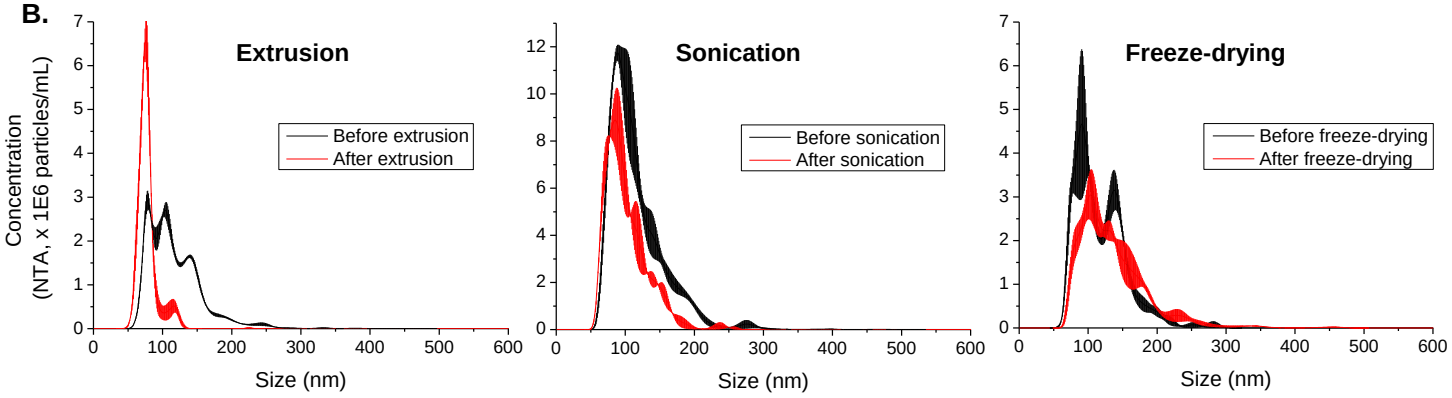


**C.**

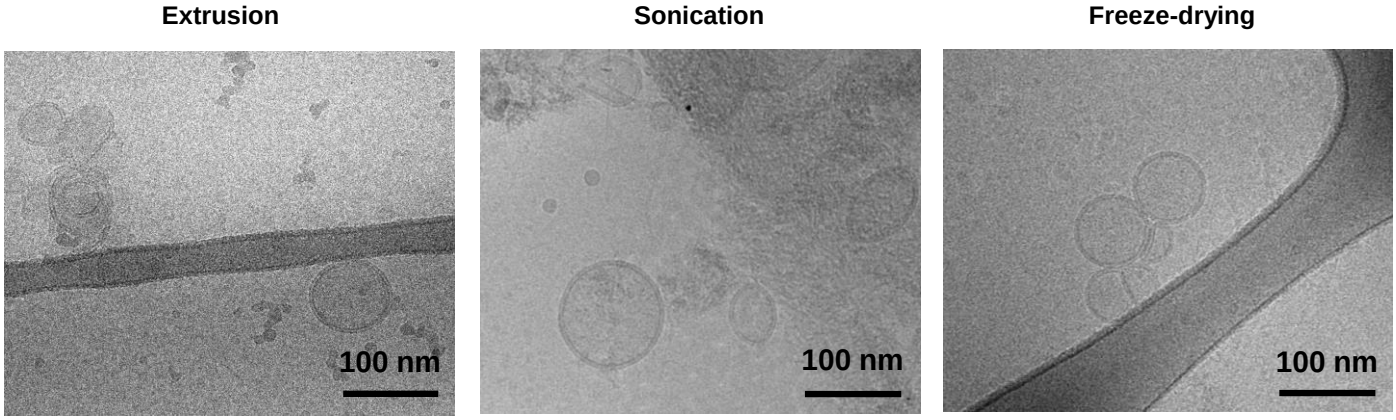


**Figure 6 – Characterisation of modified EVs.** EVs were extruded through 100 nm then 50 nm polycarbonate membranes, sonicated or freeze-dried. **A. Characterisation by NTA.** NTA analysis was performed before and after process. Results are expressed as mean ± SD of 4 (extrusion or freeze-drying) or 3 (sonication) independent experiments. Pair-sample t-tests were performed to compare mode, mean and SD before and after modification, and one-sample t-tests were performed to compare concentration after modification to 100% (before modification) (* : $p<0.05$, ** : $p<0.01$, *** : $p<0.001$). **B. NTA distribution profiles before and after modification.** Profiles are presented for one representative experiment. Results are expressed as mean ± SD of the three NTA measurements performed per sample (3 videos analysed). **C. CryoTEM analysis.**

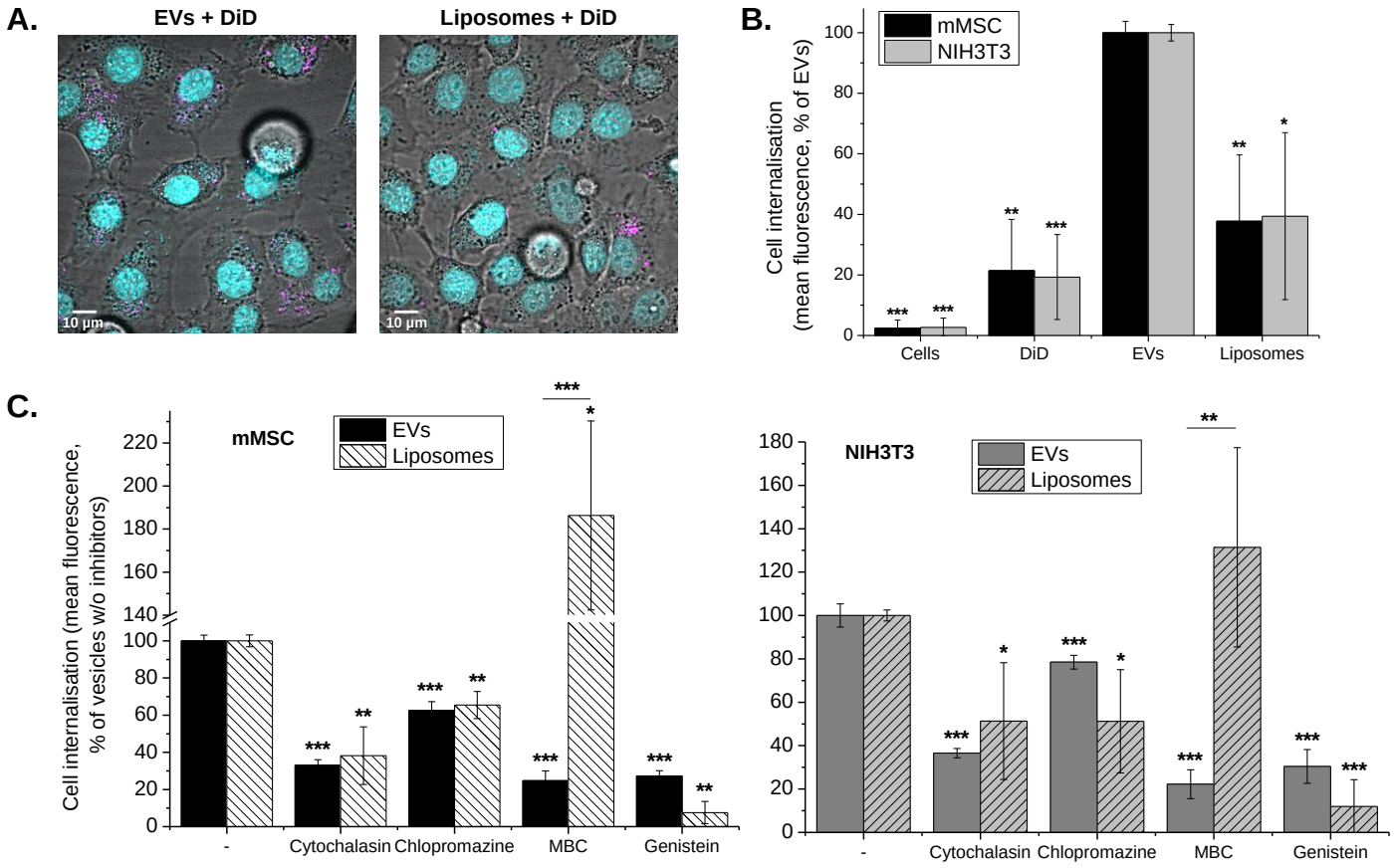


**Figure 7 – Internalisation and endocytic pathway of EVs and HSPC/Chol commercial liposomes. A. Internalisation of EVs and liposomes in NIH3T3 assessed by confocal microscopy.** Uptake of DiD-labelled EVs and liposomes ($2 \times 10^8$ vesicles for 50,000 cells) was observed. Images from transmitted, Hoechst (nuclei, in cyan) fluorescence and DiD (vesicles, in magenta) fluorescence channels were merged using Image J software. **B. Internalisation of EVs and liposomes in mMSC and NIH3T3 assessed by flow cytometry**. Uptake in producing cells (mMSC) and foreign cells (NIH3T3) of DiD-labelled EVs and liposomes ($1 \times 10^8$ vesicles for 200,000 cells) was assessed by flow cytometry. Results are expressed as a percentage of the mean fluorescence of cells incubated with labelled EVs, and as the mean ± SD of 4 independent experiments. One-sample t-tests were conducted to compare percentages to the theoretical value of 100%, which corresponds to EV internalisation in mMSC (respectively NIH3T3) (* : $p<0.05$, ** : $p<0.01$, *** : $p<0.001$). **C. Endocytic pathways followed by EVs and liposomes assessed by flow cytometry**. mMSC (left) or NIH3T3 (right) were pre-incubated with endocytic route inhibitors before addition of labelled vesicles. Results are expressed as a percentage of the mean fluorescence of labelled vesicles without (w/o) inhibitors, and as the mean ± SD of 4 independent experiments. One-sample t-tests were performed to compare percentages to the theoretical value of 100%, which corresponds to EV (respectively liposome) internalisation in the absence of inhibitors. Additionally, two-sample t-tests were performed to compare EV and liposome internalisation in the presence of MBC (* : $p<0.05$, ** : $p<0.01$, *** : $p<0.001$).

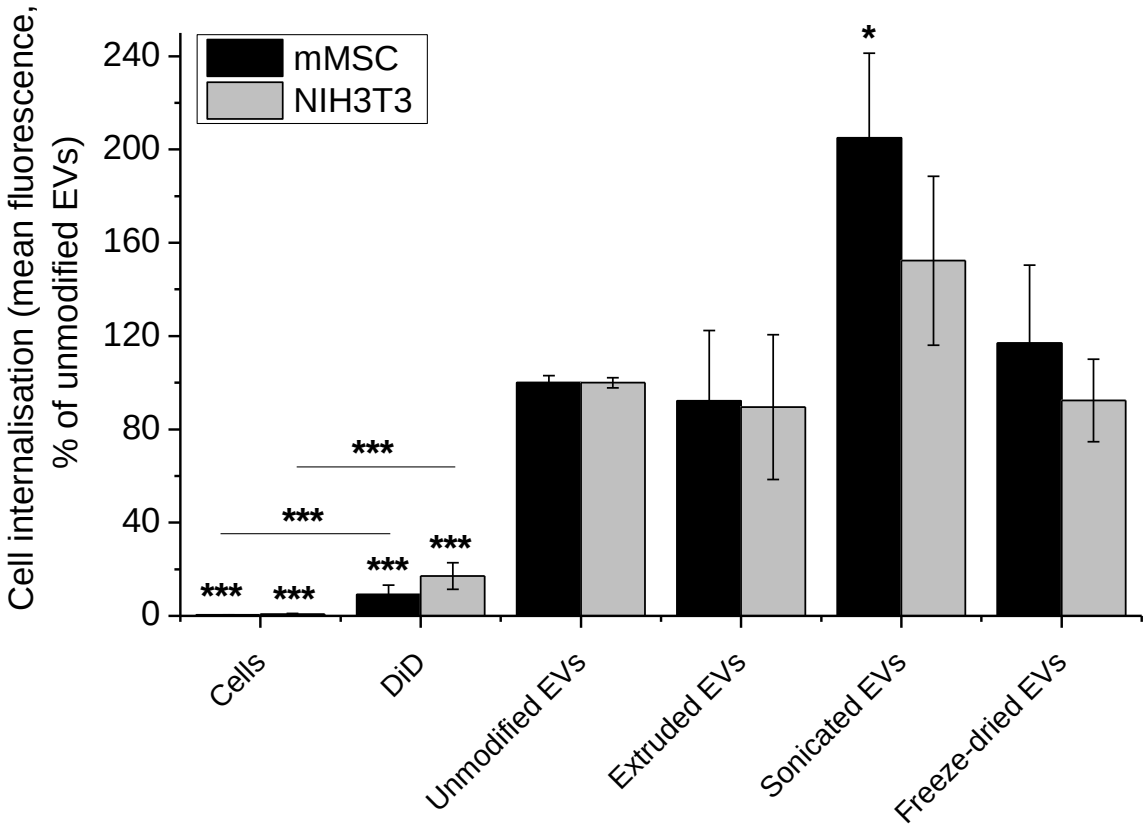


**Figure 8 – Internalisation of modified EVs.** Uptake in producing cells (mMSC) and foreign cells (NIH3T3) of DiD-labelled unmodified and modified EVs ($1 \times 10^8$ EVs for 200,000 cells) was assessed by flow cytometry. Results are expressed as a percentage of the mean fluorescence of labelled unmodified EVs, and as the mean ± SD of 3 independent experiments (or 6 experiments for cells, DiD and unmodified EVs). One-sample t-tests were performed to compare percentages to the theoretical value of 100%, which corresponds to unmodified EV internalisation in mMSC (respectively NIH3T3). Additionally, two-sample t-tests were performed to compare percentages for cells alone or treated with DiD (* : $p<0.05$, ** : $p<0.01$, *** : $p<0.001$).